1

Introduction of Microporous Membranes

1.1 Introduction

Membrane technology is widely considered as an important process and is used in a broad range of applications, such as chemical and biological processes. Membrane separation represents one of the most important applications of membrane science and technology. Membrane separation is practiced on feed streams ranging from small gases to large colloids. The key property that is exploited for gas separation is the ability of a membrane to allow a particular gas species in the gas mixture to permeate freely through the membrane while hindering the permeation of other species. In liquid separation, the goal is to control the transport rate of a colloidal particle while retaining other particles in a reservoir.

1.2 Historical Development of Membranes

Membrane science and technology has a long history, and the studies can be traced back to the eighteenth century [1]. The development of membrane technology can be divided into two periods of early membranes and modern membranes. The concept of membrane permeation was proposed in 1740s. The word *osmosis* was coined by Abbé Nolet to describe the permeation of water through a diaphragm in 1748. In the nineteenth century, theories were started in laboratory to describe the physical/chemical behaviors of membranes. For example, in 1887, the limit law was developed by van't Hoff through the measurements of solution osmotic pressure with membranes made by Traube and Pfeffer. The law was intended to explain the behavior of ideal dilute solutions, the work of which also led directly to the van't Hoff equation. Almost at the same time, the concept of a perfectly selective semipermeable membrane was used by Maxwell and others in developing the kinetic theory of gases.

Early membranes were experimented with different types of bio-diaphragm, such as animal bladders or fish casings. Later, membranes made of nitrocellulose were investigated because of reproducibility. In 1907, Bechhold devised a technique to prepare nitrocellulose membranes of graded pore size [2]. With extensive studies from other workers such as Elford [3], Zsigmondy and Bachmann [4], and Ferry, Bechhold's technique [5] was greatly improved to prepare

Microporous Materials for Separation Membranes, First Edition. Xiaoqin Zou and Guangshan Zhu.

high-quality nitrocellulose-based membranes. As a result of their efforts, microporous membranes were commercialized by the early 1930s. In the next 20 years, microporous membranes were applied to the microfiltration (MF) technology. For instance, MF membranes found their first significant application in the testing of drinking water in most Europe, particularly for Germany during the end of World War II. The research effort to develop these membranes as filters, sponsored by the US Army, was continued by the Millipore Corporation. In addition to the technique renewal, membrane materials were expanded to other polymers, such as cellulose acetate.

Modern membranes appeared during 1960s, but they are only used for laboratory purpose or small-scale industrial application. Membranes suffered from four drawbacks of unreliability, slow transport, low selectivity, and large expense, which limited their widespread use as a separation process. Solutions to each issue have been resolved, which paved way to the wide application in separation processes. The significant event was witnessed by the transformation from a laboratory to an industrial process in membrane separation. The single most important work could be counted for the Loeb–Sourirajan process for making defect-free, high-flux, anisotropic reverse osmosis (RO) membranes [6]. These membranes consist of an ultrathin, selective surface film of cellulose acetate supported on a much thicker but much more permeable porous substrate. The technical support from scientific researchers and engineers, as well as the timely infusion of financial funds for research and development from the US Department of Interior, Office of Saline Water (OSW), resulted in the commercialization of RO membranes. In parallel with industrial applications in environmental processes, the potentiality of membranes was realized for medical separation processes. The success was made in the artificial kidney, for example, Kolf and Berk [7] demonstrated the first successful artificial kidney in the Netherlands in 1945. Since the 1960s, the use of membranes in artificial organs has become a major lifesaving procedure after a longtime technology refinement. The sales of these devices comfortably dominated the membrane market, which largely exceeded that of the total industrial membrane separations. Another representative application of membranes is as blood oxygenator and controlled drug delivery system. The membrane techniques developed by ALZA (a company founded by Alex Zaffaroni) and its peers were widely used in the pharmaceutical industry to improve the efficiency and safety of drug delivery. The membrane technology is maturing in the next decade (1970s), experienced by a number of technique innovations taken place during this period. Sponsored by OSW, other membrane fabrication techniques on the basis of Loeb–Sourirajan one, including interfacial polymerization and multilayer composite casting and coating, were introduced for producing high-performance membranes. Engineering the membranes with very thin selective layers down to 0.1 μm or even less has been accomplished by several companies. Methods of packaging membranes with large areas and different configurations such as spiral wound, hollow fine fiber, capillary, and plate-and-frame modules were also developed. Improvements and advances have been made in enhancing the membrane stability. The fruits of the OSW program came out in commercial membrane units in the late 1970s, and the modern membrane technology began in the early 1980s.

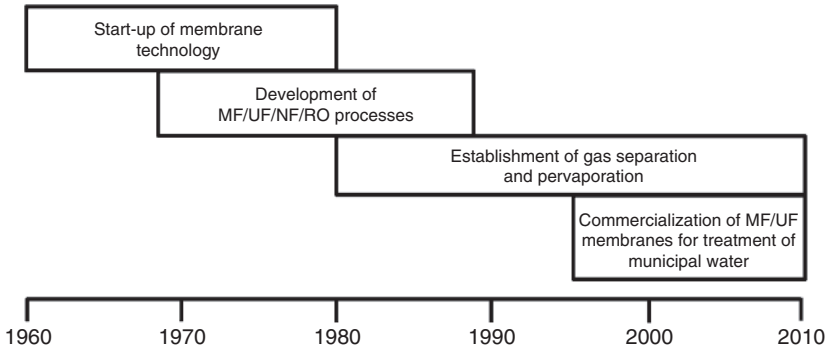

Figure 1.1 Historical development of membrane separation technology from 1960 to 2010.

The development of modern membranes can be divided into the following phases (Figure 1.1).

In the first phase, natural and synthetic polymers were employed for fabricating membranes in large scales. MF, ultrafiltration (UF), RO, and electrodialysis (ED) were well established in industries. The emergence of industrial membrane gas separation processes opened a new avenue in membrane technology. The first major product was the Monsanto Prism membrane for hydrogen separation [8]. The Dow Chemical Company started to produce membrane systems for separating nitrogen from air. Within a few years, Cynara and Separex tried to make polymeric membranes to separate carbon dioxide from natural gas. Gas separation technology is continuing to evolve and expand owing to the vast resources of polymers and matured membrane fabrication techniques. Further growth is experienced in the coming years with a milestone of pervaporation (PV) in the membrane road map. Gesellschaft für Trenntechnik (GFT), a small German engineering company, introduced the first commercial PV system for dehydration of alcohol and other solvents. Since then, a number of PV-based plants have been installed for ethanol and isopropanol dehydration, particularly for bioethanol extraction from biomass. The third development phase, which began in the mid-1990s, was the establishment of reliable and economical MF/UF membranes for the treatment of municipal water sources and for use in membrane bioreactors (MBR) in sewage treatment plants. Concurrent with the progress in polymer membranes, inorganic membranes evolved in the 1990s. Ceramic membranes represent a classic type of inorganic membranes. Artificial ceramic membranes were made from inorganic materials such as alumina, titania, zirconia oxides, silicon carbide, or some glassy materials. The first trial of ceramic membranes was employed for uranium enrichment in the nuclear industry in France in the late 1980s. After many of the nuclear plants were set up in France, other industrial application areas for the ceramic membranes were sought out. Meanwhile, academic research on ceramic membranes was conducted [9]. Most ceramic membranes manufacturers were based in France, and other companies outside France (e.g. Philips Ceramics Uden, Atech, Inopor, Jiangsu Jiuwu, LiqTech, and Mantec Technical Ceramics Ltd.) also participated in the family of manufacturing ceramic membranes. They are used in membrane

operations for liquid filtration. In contrast to polymeric membranes, they can be used in separations where aggressive media (acids, strong solvents) are present. They also have excellent thermal stability that makes them usable in high temperature membrane operations. According to the timeline of membrane development, much effort in modern times has been done to improve membrane performance by creating new materials. Around 2000s, advanced membranes made of zeolites were synthesized [10]. The advent of zeolite membranes not only enriches the diversity of inorganic membranes but also brings benefits in enhancing separation performance in terms of selectivity and permeability. More recently, microporous polymeric materials are proposed for making molecular sieving membranes because of their ordered pores and well-defined crystalline structures. Microporous materials can be catalogued into microporous silica, porous polymer, carbon, zeolites, metal–organic frameworks (MOFs), and porous organic frameworks (POFs) [11]. The scope of this book covers a wide range of topics of microporous membranes made of these materials.

1.3 Microporous Materials

In general, a solid skeleton comprising pores and/or voids is considered as a porous material. In practice, all solid materials can provide a porous medium; thus the chemical nature of porous solids is extremely rich, covering all important groups of materials: inorganic and organic crystals, carbons, polymers, glasses, ceramics, and metals. The International Union of Pure and Applied Chemistry (IUPAC) classifies porous materials according to their pore sizes: (i) microporous, with pores less than 2.0 nm; (ii) mesoporous, with pores from 2.0 to 50 nm; and (iii) macroporous, with pores between 50 and 1000 nm [12]. The pore size controls the accessibility to the pore volume, while the capacity is determined by the ratio between the skeleton and the empty space. A consequence of porous organization is the high specific surface area (SSA) of porous materials, which can vary from several hundred to several thousand square meters per gram of solid. Another important characteristic determining the properties of porous materials is their structural organization. Based on this last criterion, porous solids are divided into two major groups, that is, crystalline and amorphous. It is important to note that the properties of porous materials depend on their chemical nature. Thus, the combination of pore characteristics, structural organization, and chemical composition determines the overall property of a porous material and its possible area of application. Table 1.1 shows the different species of microporous materials according to their frameworks.

1.3.1 Carbonaceous Materials

Porous and nanostructured carbonaceous materials are very promising materials for numerous applications because of their unique pore structures, low cost, lightweight, and the abundance of natural raw materials used in their syntheses. Several classes of carbonaceous materials are discussed as follows (Figure 1.2).

Table 1.1 Microporous materials.

Categories	Various materials	Properties
Carbonaceous materials	Activated carbons, ordered mesoporous carbon, carbide derivatives	Pure carbon component, easy availability, considerable porosity, high stability
Porous organic materials	CPNs, MOFs (MOF-177, MIL-101), COFs (COF-1, COF-10, COF-108), ZIFs	Adjustable pore sizes, tunable pore surfaces, diversified skeletons
Zeolite molecular sieves	Ordered mesoporous silica, zeolite 13X, zeolite 5A, MCM-41	Uniform pore structures, inorganic components, solid acidity

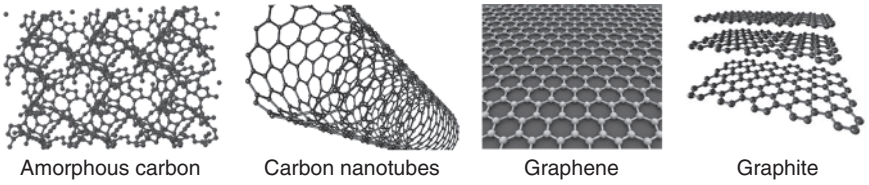

Figure 1.2 Representative classes of carbonaceous materials.

1.3.1.1 Activated Carbon

Activated carbon, also called activated charcoal, is a form of carbon processed to have small, low-volume pores that increase the surface area available for adsorption or chemical reactions. Activated carbon is carbon produced from carbonaceous source materials such as nutshells, coconut husk, peat, wood, coir, lignite, coal, and petroleum pitch. It can be produced by one of the following processes:

1. Physical activation: The source material is developed into activated carbons using hot gases. Air is then introduced to burn out the gases, creating a graded, screened, and de-dusted form of activated carbon. This is generally done by using one or a combination of the following processes:
   (i) Carbonization: Material with carbon content is pyrolyzed at temperatures in the range of 600–900 °C, usually in inert atmosphere with gases like argon or nitrogen.
   (ii) Activation/oxidation: Raw material or carbonized material is exposed to oxidizing atmospheres (oxygen or steam) at temperatures above 250 °C, usually in the temperature range of 600–1200 °C.
2. Chemical activation: Prior to carbonization, the raw material is impregnated with certain chemicals. The chemical is typically an acid, strong base, or a salt (phosphoric acid, potassium hydroxide, sodium hydroxide, calcium chloride, and zinc chloride 25%) [13]. Then, the raw material is carbonized at lower temperatures (450–900 °C). It is believed that the carbonization/activation step proceeds simultaneously with the chemical activation. Chemical activation is preferred over physical activation owing to the lower temperatures and shorter time needed for activating the material. Activated carbon may be the most widely used sorbent.

Its manufacture and use dates back to the nineteenth century. Its usefulness derives mainly from its large micropore and mesopore volumes and the resultant high surface area [14]. Activated carbon could be divided into activated carbon fibers (ACFs), activated carbon monoliths (ACMs), and powdered activated carbons (PACs), which were widely used for gas storage and separation [15], and they could be made from various precursors. Mostly, ACFs come from precursors such as polyacrylonitrile fiber, and PACs are obtained from different coal precursor anthracites or different kinds of ligneous materials such as coconut shells, grains, and bamboos. However, ACMs are made by the PACs and ACFs under high pressure and temperature or using some binders.

A gram of activated carbon can have a surface area in excess of 500 m^2 with 1500 m^2 being readily achievable. Carbon aerogels, although more expensive, have even higher surface areas and are used in special applications. Under an electron microscope, the high-surface-area structures of activated carbon are revealed. Individual particles are intensely convoluted and display various kinds of porosity; there may be many areas where flat surfaces of graphite-like materials run parallel to each other, separated by only a few nanometers or so. These micropores provide superb conditions for adsorption to occur, since the adsorbing material can interact with many surfaces simultaneously. Tests of adsorption behavior are usually done with nitrogen gas at 77 K under high vacuum, but in everyday terms activated carbon is perfectly capable of producing the equivalent, by adsorption from its environment, liquid water from steam at 100 °C and a pressure of 1 atm. Physically, activated carbon binds materials by van der Waals force or London dispersion force. Activated carbon does not bind well to certain chemicals, including alcohols, diols, strong acids and bases, metals, and most inorganics, such as lithium, sodium, iron, lead, arsenic, fluorine, and boric acid. Activated carbons can be further modified by different chemical approaches. Acid–base, oxidation–reduction, and specific adsorption characteristics are strongly dependent on the composition of the surface functional groups [16]. The surface of conventional activated carbon is reactive, capable of oxidation by atmospheric oxygen and oxygen plasma [17], steam [18], carbon dioxide [19], and ozone [20]. Oxidation in the liquid phase is caused by a wide range of reagents (HNO_3, H_2O_2, $KMnO_4$) [21]. The formation of a large number of basic and acidic groups on the surface of oxidized carbon to sorption and other properties can differ significantly from the unmodified forms [16]. Activated carbon can be nitrogenated by natural products or polymers [22] or processing of carbon with nitrogenating reagents [23]. Activated carbon can interact with chlorine [24], bromine [25], and fluorine [26]. Sulfonic acid functional groups can be attached to activated carbon to give "starbons," which can be used to selectively catalyze the esterification of fatty acids [27]. Formation of such activated carbons from halogenated precursors gives a more effective catalyst, which is thought to be a result of remaining halogens improving stability [28]. Some of the chemical properties of activated carbon have been attributed to the presence of the surface-active carbon double bond [29].

Due to high surface areas, activated carbon is used in gas purification, decaffeination, gold purification, metal extraction, water purification, medicine, sewage treatment, air filters in gas masks and respirators, filters in compressed

air, and many other applications. One major industrial application involves the use of activated carbon in the metal finishing field. It is very widely employed for purification of electroplating solutions. For example, it is a main purification technique for removing organic impurities from bright nickel plating solutions. A variety of organic chemicals are added to plating solutions for improving their deposit qualities and for enhancing properties like brightness, smoothness, ductility, etc. Due to passage of direct current and electrolytic reactions of anodic oxidation and cathodic reduction, organic additives generate unwanted breakdown products in solution. Their excessive buildup can adversely affect the plating quality and physical properties of deposited metal. Activated carbon treatment removes such impurities and restores plating performance to the desired level. Activated carbon is also used to treat poisonings and overdoses following oral ingestion. Tablets or capsules of activated carbon are used in many countries as an over-the-counter drug to treat diarrhea, indigestion, and flatulence. Carbon adsorption has numerous applications in removing pollutants from air or water streams both in the field and in industrial processes such as spill cleanup, groundwater remediation, drinking water filtration, air purification, and volatile organic compound capture from painting, dry cleaning, gasoline dispensing operations, and other processes. During early implementation of the 1974 Safe Drinking Water Act in the United States, EPA officials developed a rule that proposed requiring drinking water treatment systems to use granular activated carbon (GAC). Because of its high costs, the so-called GAC rule encountered such strong opposition all across the country from the water supply industry, including the largest water utilities in California; thus the agency set aside the rule [30]. Research is being done testing the ability of various activated carbons to store natural gas and hydrogen gas. The porous material acts like a sponge for different types of gases. The gas is attracted to the carbon material via van der Waals forces. Some carbons have been able to achieve bonding energies of 5–10 kJ mol^{-1}. The gas may then be desorbed when subjected to higher temperatures and either combusted to do work or in the case of hydrogen gas extracted for use in a hydrogen fuel cell. Gas storage in activated carbons is an appealing gas storage method because the gas can be stored in a low-pressure, low-mass, low-volume environment that would be much more feasible than bulky onboard compression tanks in vehicles. The US Department of Energy has specified certain goals to be achieved in the area of research and development of nanoporous carbon materials, such as to satisfy the goal of the ALL-CRAFT program. Filters with activated carbon are usually used in compressed air and gas purification to remove oil vapors, odor, and other hydrocarbons from the air. The most common designs use a one-stage or two-stage filtration principle in which activated carbon is embedded inside the filter media. Activated carbon is also used in spacesuit primary life support systems. Activated carbon filters are used to retain radioactive gases within the air vacuumed from a nuclear boiling water reactor turbine condenser. The large charcoal beds adsorb these gases and retain them while they rapidly decay to nonradioactive solid species. The solids are trapped in the charcoal particles, while the filtered air passes through.

1.3.1.2 Carbon Nanotubes

Carbon nanotubes (CNTs) are allotropes of carbon with cylindrical pore structures [31]. Nanotubes are members of the fullerene structural family. Their name is derived from their long, hollow structure with the walls formed by one-atom-thick sheets of carbon, called graphene. These sheets are rolled at specific and discrete angles, and the combination of the rolling angle and radius decides the nanotube properties, for example, metallic or semiconducting properties of the individual nanotube shell. Nanotubes are categorized as single-walled nanotubes (SWNTs) and multiwalled nanotubes (MWNTs). Individual nanotubes naturally align themselves into ropes held together by van der Waals forces, more specifically π-stacking. The chemical bonding in nanotubes is composed entirely of sp^2 bonds, similar to those of graphite. These bonds, which are stronger than the sp^3 bonds found in alkanes and diamond, endow nanotubes with their unique strengths. SWNTs have outer diameters in the range of 1.0–3.0 nm with inner diameters of 0.4–2.4 nm. MWNTs can have outer diameters ranging from approximately 2.0 nm (double-walled nanotubes) up to approximately 100 nm with tens of walls. Recently, three-dimensional (3D) CNT architectures based on CNTs have been also highlighted for macroscopic all-carbon devices. For instance, Lalwani et al. have reported a novel radical-initiated thermal cross-linking method to fabricate macroscopic, free-standing, porous, all-carbon scaffolds using single-walled carbon nanotubes (SWCNTs) and multiwalled carbon nanotubes as building blocks [32]. These scaffolds possess macro-, micro-, and nanostructured pores, and the porosity can be tailored for specific applications. These 3D all-carbon scaffolds may be used for the fabrication of the next generation of energy storage, supercapacitors, field emission transistors, high-performance catalysis, photovoltaics, and biomedical devices and implants [33].

Techniques have been developed to produce nanotubes in sizable quantities, including arc discharge, laser ablation, high-pressure carbon monoxide disproportionation, and chemical vapor deposition (CVD). Most of these processes take place in a vacuum or with process gases. The CVD growth method is popular, as it yields high purity and has a high degree of control over diameter, length, and morphology. Using particulate catalysts, large quantities of nanotubes can be synthesized by these methods; advances in catalysis and continuous growth are making CNTs more commercially viable [34]. Vertically aligned CNT arrays are also grown by thermal CVD. A substrate (quartz, silicon, stainless steel, etc.) is coated with a catalytic metal (Fe, Co, Ni) layer. Typically that layer is iron and is deposited via sputtering to a thickness of 1.0–5.0 nm. A 10–50 nm underlayer of alumina is often also put down on the substrate first. This imparts controllable wetting and good interfacial properties. When the substrate is heated to the growth temperature (~700 °C), the continuous iron film breaks up into small islands, and each island then nucleates a CNT. The sputtered thickness controls the island size, and this in turn determines the nanotube diameter. Thinner iron layers drive down the diameter of the islands, and they drive down the diameter of the nanotubes grown. The amount of time that the metal island can sit at the growth temperature is limited, as they are mobile and can merge into larger (but fewer) islands. Annealing

at the growth temperature reduces the site density (CNT number mm^{-2}) while increasing the catalyst diameter. CNTs can be functionalized to attain desired properties that can be used in a wide variety of applications. The two main methods of CNT functionalization are covalent and non-covalent modifications. Because of their hydrophobic nature, CNTs tend to agglomerate, hindering their dispersion in solvents or viscous polymer melts. The resulting nanotube bundles or aggregates reduce the mechanical performance of the final composite. The surface of the CNTs can be modified to reduce the hydrophobicity and improve interfacial adhesion to a bulk polymer through chemical attachment [35].

CNTs are the strongest and stiffest materials discovered in terms of tensile strength and elastic modulus, respectively. This strength results from the covalent sp^2 bonds formed between the individual carbon atoms. In 2000, a multiwalled carbon nanotube was tested to have a tensile strength of 63 GPa [36]. Further studies, such as one conducted in 2008, revealed that individual CNT shells have strengths of up to 100 GPa, which is in agreement with quantum/atomistic models [37]. Under excessive tensile strain, the tubes will undergo plastic deformation, which means the deformation is permanent. This deformation begins at strains of approximately 5.0% and can increase the maximum strain the tubes undergo before fracture by releasing strain energy. Although the strength of individual CNT shells is extremely high, weak shear interactions between adjacent shells and tubes lead to significant reduction in the effective strength of multiwalled carbon nanotubes and CNT bundles down to only several GPa [38]. This limitation has been recently addressed by applying high-energy electron irradiation, which cross-links inner shells and tubes and effectively increases the strength of these materials to approximately 60 GPa for multiwalled carbon nanotubes [37] and approximately 17 GPa for double-walled CNT bundles [38]. The surface wettability of CNT is of importance for its applications in various settings. Although the intrinsic contact angle of graphite is around 90°, the contact angles of most as-synthesized CNT arrays are over 160°, exhibiting a superhydrophobic property. By applying a voltage as low as 1.3 V, the extreme water-repellent surface can be switched to a superhydrophilic one [39]. Another characteristic of CNTs is their unique electrical properties. Unlike two-dimensional (2D) graphene, CNTs are either metallic or semiconducting along the tubular axis. For a given (n, m) nanotube, if $n = m$, the nanotube is metallic; if ($n - m$) is a multiple of 3, then the nanotube is semiconducting with a very small band gap. Otherwise the nanotube is a moderate semiconductor. Thus, all armchair ($n = m$) nanotubes are metallic, and nanotubes (6, 4), (9, 1), etc. are semiconducting [40]. CNTs are not semimetallic because the degenerate point (the point at zero energy where bonding π-band meets antibonding π*-band) is slightly shifted away from the K point in the Brillouin zone due to the curvature of the tube surface, causing hybridization between the σ^* and π^* antibonding bands and then modifying the band dispersion. Some exceptions also exist regarding metallic versus semiconductor behavior, because curvature effects in small diameter tubes can strongly influence electrical properties. For instance, a (5, 0) SWCNT that should be semiconducting in fact is metallic according to the calculations. Likewise, zigzag and chiral SWCNTs with small

diameters that should be metallic have a finite band gap. In theory, metallic nanotubes can carry an electric current density of 4×10^9 A cm^{-2}, which is more than 1000 times greater than those of metals such as copper, because copper interconnect current densities are limited by electromigration [41]. CNTs are being explored as conductivity-enhancing components in composite materials, and many groups are attempting to commercialize highly conducting electrical wire assembled from individual CNTs. There are still some challenges to be overcome, such as reducing resistive nanotube-to-nanotube junctions and impurities, because they lower the electrical conductivity of the macroscopic nanotube wires by orders of magnitude compared with the conductivity of the individual nanotubes. Because of its nanoscale cross section, electrons propagate only along the tube's axis. As a result, CNTs are frequently referred to as one-dimensional (1D) conductors. The maximum electrical conductance of an SWCNT is $2G_0$ ($G_0 = 2e^2\ h^{-1}$, a conductance of a single ballistic quantum channel) [42]. Due to the π-electron system in determining the electronic properties of graphene, doping in CNTs differs from that of the same group of crystalline semiconductors (e.g. silicon). Graphitic substitution of carbon atoms in the nanotube wall by boron or nitrogen dopants leads to p-type and n-type behavior, respectively. However, some non-substitutional (intercalated or adsorbed) dopants introduced into a CNT, such as alkali metals as well as electron-rich metallocenes, result in n-type conduction because they donate electrons to the π-electron system of the nanotube. In contrast, π-electron acceptors such as $FeCl_3$ or electron-deficient metallocenes function as p-type dopants since they draw π-electrons away from the top of the valence band.

Current use and application of nanotubes has mostly been limited to the use of bulk nanotubes, which is a mass of rather unorganized fragments of nanotubes. Bulk nanotube materials may never achieve a tensile strength similar to that of individual tubes, but such composites may, nevertheless, yield strengths sufficient for many applications. Bulk CNTs have already been used as composite fibers in polymers to improve the mechanical, thermal, and electrical properties of the bulk product. Easton-Bell Sports Inc. has been in partnership with Zyvex Performance Materials, using CNT technology in a number of their bicycle components including flat and riser handlebars, cranks, forks, seat posts, stems, and aero bars. Zyvex Technologies has also built a 54′ maritime vessel (Piranha Unmanned Surface Vessel), as a technology demonstrator for CNT technology. CNTs help improve the structural performance of this vessel, resulting in a lightweight 8000 lb boat that can carry a payload of 15 000 lb over 2500 miles. Amroy Europe Oy manufactures Hybtonite carbon nanoepoxy resins, where CNTs have been chemically activated to bond to epoxy, resulting in a composite material that is 20–30% stronger than other composite materials. It has been used for wind turbines, marine paints, and a variety of sports gear such as skis, ice hockey sticks, baseball bats, hunting arrows, and surfboards. Other current applications include tips for atomic force microscope probes in tissue engineering. CNTs can act as scaffolding for bone growth [43]. There is also ongoing research in using CNTs as a scaffold for diverse microfabrication techniques [44]. The strength and flexibility of CNTs makes them of potential use in controlling other nanoscale structures, suggesting their importance in nanotechnology

engineering. Recently, several studies have highlighted the prospect of using CNTs as building blocks to fabricate 3D macroscopic all-carbon devices. For example, CNT-based yarns are suitable for applications in energy and electrochemical water treatment when coated with an ion-exchange membrane [45]. Also, CNT-based yarns could replace copper as a winding material. Pyrhönen et al. in 2015 have built a motor using CNT winding [46].

1.3.1.3 Graphene

Graphene is a 2D carbon with atomic-scale and hexagonal lattice. It is the basic structural element of other allotropes, including graphite, charcoal, CNTs, and fullerenes. It can be considered as an indefinitely large aromatic molecule. Each atom has four bonds, one σ-bond with each of its three neighbors and one π-bond that is oriented out of plane. The atoms are about 1.42 Å apart [47]. Graphene's hexagonal lattice can be regarded as two interleaving triangular lattices. In structure, graphene possesses tightly packed carbon atoms and a sp^2 orbital hybridization – a combination of orbitals s, p_x, and p_y that constitute the σ-bond. The final p_z electron makes up the π-bond. The π-bonds hybridize together to form the π-band and π*-bands. Multiple production techniques have been developed [48]. In 2014, exfoliation produced graphene with the lowest number of defects and highest electron mobility [49]. Geim and Novoselov initially used adhesive tape to pull graphene sheets away from graphite. Achieving single layers typically requires multiple exfoliation steps. After exfoliation the flakes are deposited on a silicon wafer. Crystallites larger than 1 mm and visible to the naked eye can be obtained [50]. Alternatively a sharp single-crystal diamond wedge cleaves layers from a graphite source [51]. Rapid heating of graphite oxide and exfoliation yields highly dispersed carbon powder with a few percent of graphene flakes. Another method is reduction of graphite oxide monolayer films, e.g. by hydrazine with annealing in argon/hydrogen with an almost intact carbon framework that allows efficient removal of functional groups [52]. Burning a graphite oxide produced a conductive graphene film (1738 S m^{-1}) with an SSA of 1520 m^2 g^{-1} [53]. Dispersing graphite in a liquid medium can produce graphene by sonication followed by centrifugation [54], producing a concentration of 2.1 mg ml^{-1} in *N*-methylpyrrolidone [55]. Using a suitable ionic liquid as the dispersing liquid medium produced a concentration of 5.33 mg ml^{-1} [56]. Restacking is an issue with this technique. Adding a surfactant to a solvent prior to sonication prevents restacking by adsorbing to the graphene surface. This produces a higher graphene concentration, but removing the surfactant requires chemical treatments. Sonicating graphite at the interface of two immiscible liquids, most notably heptane and water, produced macroscale graphene films. The graphene sheets are adsorbed to the high-energy interface between the materials and are kept from restacking. The sheets are up to about 95% transparent and conductive [57]. Graphene can be produced by CVD. Growing graphene in an industrial resistive heating cold wall CVD system was claimed to produce graphene 100 times faster than conventional CVD systems, cutting costs by 99% and producing material with enhanced electronic qualities [58]. Cold wall CVD technique can be used to study the underlying surface science involved in graphene nucleation and growth as it allows control of

process parameters like gas flow rates, temperature, and pressure. A homebuilt vertical cold wall system uses resistive heating by passing direct current through the substrate. It provides insight into a typical surface-mediated nucleation and growth mechanism involved in 2D materials grown using catalytic CVD under conditions sought out in the semiconductor industry [59]. Microwave energy was reported to directly synthesize graphene in one step [60]. This approach avoids use of potassium permanganate in the reaction mixture. Microwave radiation assistance allows the synthesis of graphene oxide with or without holes by controlling microwave time [61]. Microwave heating can dramatically shorten the reaction time from days to seconds.

Graphene has many unusual properties. It is about 200 times stronger than the strongest steel. It efficiently conducts heat and electricity and is nearly transparent [62]. It also shows a large and nonlinear diamagnetism. It has a theoretical SSA of 2630 $m^2\ g^{-1}$. This is much larger than that reported to date for carbon black (typically smaller than 900 $m^2\ g^{-1}$) or for CNTs, from approximately 100 to 1000 $m^2\ g^{-1}$, and is similar to activated carbon [63]. The most important property of graphene is its electronic behavior. Graphene is a zero-gap semiconductor, because its conduction and valence bands meet at the Dirac points. The Dirac points are six locations in momentum space, on the edge of the Brillouin zone, divided into two non-equivalent sets of three points. The two sets are labeled K and K′. The sets give graphene a valley degeneracy of $g\nu = 2$. Four electronic properties such as electronic spectrum, dispersion relation, single-atom wave propagation, and electron transport separate it from other condensed matter systems. The most studied property is electron transport. Graphene displays remarkable electron mobility at room temperature, with reported values in excess of 15 000 $cm^2\ V^{-1}\ s^{-1}$. Hole and electron mobility was expected to be nearly identical [64]. The mobility is nearly independent of temperature between 10 and 100 K [65], which implies that the dominant scattering mechanism is defect scattering. Scattering by graphene's acoustic phonons intrinsically limits room temperature mobility to 200 000 $cm^2\ V^{-1}\ s^{-1}$ at a carrier density of $10^{12}\ cm^{-2}$, 10^7 times greater than copper [66]. The corresponding resistivity of graphene sheets would be $10^{-6}\ \Omega$ cm. This is less than the resistivity of silver, the lowest otherwise known at room temperature. However, on SiO_2 substrates, scattering of electrons by optical phonons of the substrate is a larger effect than scattering by graphene's own phonons. This limits mobility to 40 000 $cm^2\ V^{-1}\ s^{-1}$. Charge transport is affected by adsorption of contaminants such as water and oxygen molecules. This leads to non-repetitive and large hysteresis I–V characteristics. Graphene surfaces can be protected by a coating with materials such as SiN, PMMA, or h-BN. In 2015, lithium-coated graphene was observed to exhibit superconductivity, and in 2017 evidence for unconventional superconductivity was demonstrated in single-layer graphene placed on the electron-doped (non-chiral) *d*-wave superconductor [67]. Electrical resistance in 40 nm wide nanoribbons of epitaxial graphene changes in discrete steps. The ribbon conductance exceeds predictions by a factor of 10. The ribbons can act more like optical waveguides or quantum dots, allowing electrons to flow smoothly along the ribbon edges [68]. Transport is generally dominated by two modes: one is ballistic and temperature independent, and

the other is thermally activated. Ballistic electrons resemble those in cylindrical CNTs. At room temperature, resistance increases abruptly at a particular length (the ballistic mode at 16 mm and the other at 160 nm). Graphene electrons can cover micrometer distances without scattering, even at room temperature [69]. Despite zero carrier density near the Dirac points, graphene exhibits a minimum conductivity on the order of $4e^2\ h^{-1}$. The origin of this minimum conductivity is unclear. However, rippling of the graphene sheet or ionized impurities in the SiO_2 substrate may lead to local puddles of carriers that allow conduction. Several theories suggest that the minimum conductivity should be $4e^2\ (\pi h)^{-1}$; however, most measurements are at an order of $4e^2\ h^{-1}$ or greater and depend on impurity concentration [70]. Near zero carrier density graphene exhibits positive photoconductivity and negative photoconductivity at high carrier density. This is governed by the interplay between photoinduced changes of both Drude weight and carrier scattering rate. Graphene doped with various gaseous species (both acceptors and donors) can be returned to an un-doped state by gentle heating in vacuum [71]. Even for dopant concentrations in excess of $10^{12}\ cm^{-2}$, carrier mobility exhibits no observable change. Graphene doped with potassium in ultrahigh vacuum at low temperature can reduce mobility about 20-fold [72]. The mobility reduction is reversible on removing potassium. Due to graphene's two dimensions, charge fractionalization (where the apparent charge of individual pseudoparticles in low-dimensional systems is less than a single quantum) [73] is thought to occur. It may therefore be a suitable material for constructing quantum computers [74] using anyonic circuits [75]. Thermal transport in graphene is an active area of research that has attracted attention because of the potential for thermal management applications. Early measurements of the thermal conductivity of suspended graphene reported an exceptionally large thermal conductivity of approximately $5300\ W\ m^{-1}\ K^{-1}$ [76], compared with the thermal conductivity of pyrolytic graphite of approximately $2000\ W\ m^{-1}\ K^{-1}$ at room temperature [77].

Graphene is the only form of carbon (or solid material) in which every atom is available for chemical reaction from two sides. Atoms at the edges of a graphene sheet have special chemical reactivity. Graphene has the highest ratio of edge atoms of any allotrope. Defects within a sheet increase its chemical reactivity [78]. The onset temperature of reaction between the basal plane of single-layer graphene and oxygen gas is below 260 °C [79]. Graphene combusts at 350 °C [80]. Graphene is commonly modified with oxygen- and nitrogen-containing functional groups and analyzed by infrared spectroscopy and X-ray photoelectron spectroscopy. However, determination of structures of graphene with oxygen- [81] and nitrogen-containing [82] functional groups requires the structures to be well controlled. Single-layer graphene is a 100 times more chemically reactive than thicker sheets. Graphene placed on a soda-lime glass (SLG) substrate under ambient conditions exhibited spontaneous n-doping ($1.33 \times 10^{13}\ e\ cm^{-2}$) via surface transfer. On p-type copper indium gallium selenide (CIGS) semiconductor itself deposited on SLG, n-doping reached $2.11 \times 10^{13}\ e\ cm^{-2}$ [83].

Graphene is a transparent and flexible conductor that holds great promise for various material or device applications, including solar cells, light-emitting diodes (LED), touch panels, and smart windows or phones [84, 85]. China-based

2D Carbon Graphene Material Co., Ltd. has sold graphene-based touch panel modules in volume to cell phone, wearable device, and home appliance manufacturers. For instance, smartphone products with graphene touch screens are already on the market. In 2013, Head announced their new range of graphene tennis racquets. In 2015, one product of graphene-infused printer was available for commercial use. In 2016, researchers made a graphene film that can absorb 95% of light incident. Graphene is often produced as a powder and as dispersion in a polymer matrix. This dispersion is supposedly suitable for advanced composites, paints and coatings, lubricants, oils and functional fluids, capacitors and batteries, thermal management applications, display materials and packaging, solar cells, inks, and 3D printers [86]. Many other uses for graphene have been proposed or are under development in the diverse areas including electronics, biological engineering, filtration, lightweight/strong composite materials, photovoltaics, and energy storage [87].

1.3.2 Microporous Silica

Microporous silica is an inorganic material with an amorphous structure in a wide temperature range and is able to be sintered in dry atmosphere at temperatures around 400–700 °C. Microporous silica contains high porosities and exceptionally small pores showing molecular sieving characteristics. There are several synthesis methods for producing microporous silica, including sol–gel, templating approach, and CVD. Among these methods, sol–gel processing attracts most attention due to its excellent processability, its potential to precisely control pore size and pore structure, and its ease of scaling up in industry [88]. Sol–gel synthesis processes are divided into three main procedures: (1) polymeric route and slip casting, (2) the route of colloidal sol and hot coating, and (3) the surfactant-templated method. There are two main types of colloidal and polymeric sol–gel routes that can be distinguished. In the colloidal route, the elemental unit is a solid nanoparticle dispersed as stable sol in a liquid. The sol stability is related to electrostatic and steric repulsive interactions [89]. Hydrolysis and condensation reaction is fast in the colloidal route, resulting in a fully hydrolyzed oxide. This rapid condensation process causes particulate growth or the formation of precipitates [90]. The fast precipitation usually leads to dense silica phase. In comparison with colloidal route, the polymeric route is the most convenient way for preparation of microporous silica from solutions of molecular precursors like alkoxides, because alkoxy group can serve as porogen in creating pores in silica compounds. Typically in the polymeric route, the elemental unit that is usually a silicon alkoxide, $Si(OR)_4$, is initially used as a molecular precursor. The most common precursors include tetramethyl orthosilicate ($Si(OCH_3)_4$) (TMOS) and tetraethyl orthosilicate ($Si(OC_2H_5)_4$) (TEOS) in solution in their associated alcohols. The polymeric gel synthesis consists of hydrolysis and condensation reactions, which can be either acid or base catalyzed. However, base-catalyzed synthesis does not result in microporous materials due to large and highly cross-linked particles, whereby only acid-catalyzed reactions will result in microporous materials. Figure 1.3 shows a graphical summary of sol–gel process of microporous silica from molecular

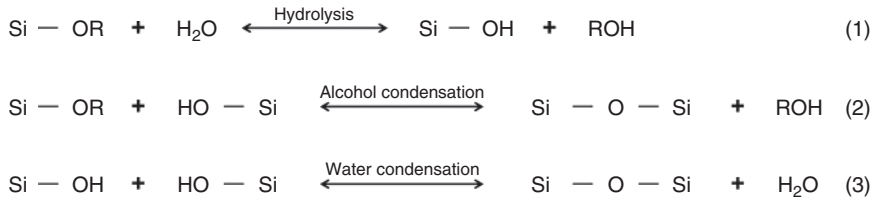

Figure 1.3 Sol–gel process for the formation of silica polymers.

solutions. (1) and (3) show the synthesis of silica polymers by sol–gel process involving hydrolysis and condensation reactions of starting alkoxides [91].

For preparation of microporous silica, good manipulation either on silanol hydrolysis or polysilicate condensation is very important. For instance, in the acid catalytic system of polymeric sol route, the hydrolysis reaction is kept slower and typically achieved by adding a small amount of water, resulting in a partially hydrolyzed alkoxide and the formation of a linear inorganic polymer. Through the subsequent gelation process, polymeric sols form a gel network. By controlling the reactant concentrations and the synthesis conditions, the sol–gel morphology can be changed. This is achieved by the control of rates of hydrolysis and condensation by changing amount of water or catalyst used. The structure of the resulting polymers could change from linear to weakly branched polymers. Short branched linear polymers are the most preferred for formation of microporous silica membranes [91]. The characteristics of sol–gel-derived silica are determined by a large number of sol–gel process parameters. Variation of one or more parameters such as pH of the solution, reaction temperature, and water–silica ratios can dramatically affect the microstructure of the resulting silica [92]. Therefore, it is important that the effects of these parameters are well understood to make sol–gel process a reliable and practical technology for membrane fabrication [93]. Besides having great advantage of pore size control based on starting precursors and size of silica sols, sol–gel processing also allows for low temperature synthesis of hybrid silica compounds, such as mixed oxides by mixing metal ions into the silica matrix [94]. The insertion of metal cations into the silica framework can be attained either by a post-synthesis treatment or by the *in situ* mixing of the adequate precursors in the initial reacting systems.

Templating approach can also be applied to control the microporosity of the silica. The first strategy consists of using templating molecules (incorporated in the gelation medium), which are inert toward the chemical process leading to the inorganic network. A second approach consists of using the modified alkoxides where a molecular group acting as a template is covalently bonded to the Si atom. The synthesis conditions are selected in order to directly associate the porosity of the final materials with the thermal elimination of the templating species. There are mainly two types of templates that have been used for tailoring porous structures, i.e. surfactant molecules and organic ligands/polymers. Surfactant molecules incorporated in the matrix could arrange matrix molecules around them by means of non-covalent interactions. The thermal elimination of the template then leaves a residual porosity in the silica. Thus, the control of shape and pore size could be easily achieved by this method. The same case goes

for organic ligands/polymers; however, they are different in the sense that they are bonded covalently to the siloxane matrix [95]. Wang et al. adopted templated approach to fabricate microporous hollow silica using nonionic surfactant nonyl phenol ethoxylated decylether (NP-10) micelles as template, *n*-octadecane as core, and sodium silicate as silica precursor [96]. The core materials were removed by ethanol during the reaction; thus, the hollow silica can be formed without calcination or chemical etching. Eswaramoorthy et al. also synthesized hexagonal microporous silica employing a short-chain amine as the template molecule and have succeeded in obtaining these materials with well-defined pore distributions between 1.0 and 2.0 nm [97]. The surface area of SiO_2 after removal of the template by calcination is 800 m^2 g^{-1}. Guo et al. have synthesized uniform hollow microporous silica spheres using polystyrene spheres and cetyltrimethylammonium bromide as co-templates at room temperature in concentrated aqueous ammonia [98]. In order to have template approach successfully implemented, the following criteria must be satisfied: (i) the templating molecules must be uniformly incorporated in the inorganic matrix without aggregation or phase separation to avoid creating pores larger than the size of individual templating molecules, (ii) the synthesis and processing conditions should result in dense embedding matrix so that pores are created only by template removal, and (iii) template removal should be achieved without collapse of the matrix so that the created pores preserve the original size and shape of the template [99].

CVD is another way of producing microporous silica, usually a membrane or film on a particular substrate. It could be effectively applied for the deposition of silicon oxide or metal oxide on porous substrates in order to modify their porous structures. The CVD technique consists of the thermal decomposition of a silicon-based precursor and the chemical reaction with an oxidant gas in contact with a hot substrate. The gaseous precursors are mainly TEOS and TMOS fed to the hot surface by argon or nitrogen as carrier gas. Other possible precursors include silicon tetrachloride ($SiCl_4$) or silane (SiH_4), whereas oxidant gases are air, pure O_2, O_3, N_2O, or water vapor [100].

1.3.3 Zeolites

According to the classical definition, a zeolite is a crystalline and microporous aluminosilicate mineral [101]. The basic framework of a zeolite is built of adjacent silicon and aluminum tetrahedron forming channels/pores of microporous dimensions, where alkali or alkali-earth cations (e.g. Na^+, K^+, Ca^{2+}, Mg^{2+}) and water molecules are situated (Figure 1.4). These positive ions are rather loosely held and can readily be exchanged for others in a contact solution. The formula of natrolite, an example of zeolite, is $Na_2Al_2Si_3O_{10}{\cdot}2H_2O$.

The term zeolite was originally coined in 1756 by Swedish mineralogist Axel Fredrik Cronstedt, who discovered the first zeolite mineral [102]. Natural zeolites form where volcanic rocks and ash layers react with alkaline groundwater. Zeolites also crystallize in post-depositional environments over periods ranging from thousands to millions of years in shallow marine basins. Naturally occurring zeolites are rarely pure and are contaminated to varying degrees by other

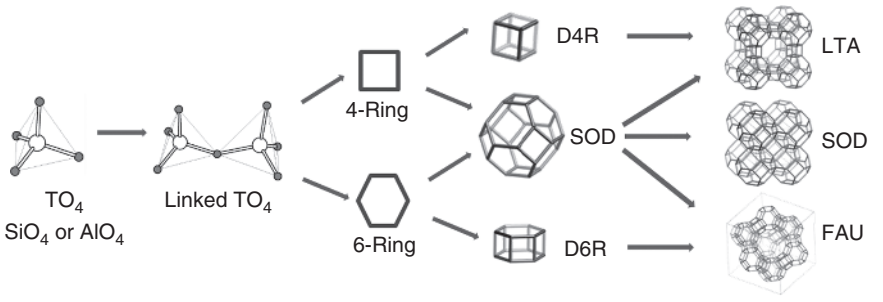

Figure 1.4 The formation process of some representative zeolites.

minerals, metals, quartz, or other zeolites. Later in 1862, the first synthetic analogue of natural zeolite was obtained [103]. Early developments took place in the mid-twentieth century, and the flourishing period in zeolite science and practice started in the early 1960s. Applications of these materials began after discovering that they can be obtained from very reactive initial systems under relatively mild hydrothermal conditions. Extensive work in industrial and academic laboratories resulted in the preparation of synthetic counterparts of zeolite minerals and new framework types that did not exist naturally. Further, organic cations that allow raising the Si/Al ratio in the zeolite framework and synthesis of new framework topology were employed in zeolite crystallization. This approach allowed the synthesis of the first high-silica zeolite, named Beta [104]. Sorption, catalytic, and ion-exchange properties of different types of zeolites were systematically studied. Most of these developments were prompted by R. M. Barrer and D. W. Breck, the founders of modern zeolite science [105]. This period was also marked by the application of zeolites in fluid catalytic cracking. The replacement of amorphous aluminosilicate catalysts by zeolite Y led to a revolution in catalytic cracking in terms of conversion and selectivity [106]. In the 1970s, a very large number of organic molecules were tested as structure-directing agents in zeolite crystallization, which resulted in the synthesis of many new structure types and the preparation of high-silica and all-silica zeolites [107]. The most important discovery in the 1980s was the development of a new family of silica-free zeolite-like materials. Aluminophosphate analogues first synthesized by Union Carbide researchers were further extended to silicon- and metal-containing counterparts including Ti, Sn, Zn, and so on [108]. The number of microporous zeolite-type structures increases every year due to synthetic advancements. As of September 2016, 232 unique zeolite frameworks have been identified, and over 40 naturally occurring zeolite frameworks are known [109]. The advances in synthesis have also allowed zeolite framework compositions to be stretched far beyond the limits observed in nature. At present the portfolio of microporous materials with well-defined periodic structures and various chemical compositions is large.

Zeolites occur naturally but are also produced industrially on a large scale. Conventional open-pit mining techniques are used to mine natural zeolites. The overburden is removed to allow access to the ore. The ore may be blasted or stripped for processing by using tractors equipped with ripper blades and front-end loaders. In processing, the ore is crushed, dried, and milled. The milled ore may be

air-classified as to particle size and shipped in bags or bulk. The crushed product may be screened to remove fine material when a granular product is required, and some pelletized products are produced from fine material. Industrially important zeolites are produced synthetically. Synthetic zeolites hold some key advantages over their natural analogues. The synthetic materials are manufactured in a uniform and phase-pure state. It is also possible to produce zeolite structures that do not appear in nature. Zeolite LTA is a well-known example. Since the principal raw materials used to manufacture zeolites are silica and alumina, which are among the most abundant mineral components on earth, the potential to supply zeolites is virtually unlimited. There are over 200 synthetic zeolites that have been synthesized by a process of slow crystallization of a silica-alumina gel in the presence of alkalis and organic templates [110]. The research is ongoing to understand the chemistry that would allow us to make theoretically predicted structures. In addition to variations in structures, zeolites can also be made with a variety of other atoms in them to make them chemically interesting and active. Some examples of the so-called heteroatoms that have been incorporated include germanium, iron, gallium, boron, zinc, tin, and titanium [111]. One of the important processes used to carry out zeolite synthesis is sol–gel processing. The product properties depend on reaction mixture composition, pH of the system, operating temperature, pre-reaction seeding/aging time, reaction time, and the templates used. In sol–gel process, other elements (metals, metal oxides) can be easily incorporated. The silicalite sol formed by the hydrothermal method is very stable. The ease of scaling up this process makes it a favorite route for zeolite synthesis.

Zeolites are known as molecular sieves, referring to a particular property of these materials, i.e. the ability to selectively sort molecules based primarily on a size exclusion process. This is due to a very regular pore structure of molecular dimensions. The maximum size of the molecular or ionic species that can enter the pores of a zeolite is controlled by the dimensions of the channels. These are conventionally defined by the ring size of the aperture, where, for example, the term eight-ring refers to a closed loop that is built from eight tetrahedrally coordinated silicon (or aluminum) atoms and eight oxygen atoms. These rings are not always perfectly symmetrical due to a variety of effects, including strain induced by the bonding between units that are needed to produce the overall structure, or coordination of some of the oxygen atoms of the rings to cations within the structure. Due to the regularity of pores or voids, they have found widespread applications in industrial processes [112]. Zeolites are widely used as ion-exchange beds in domestic and commercial water purification, softening, and other applications. In chemistry, zeolites are used to separate molecules (only molecules of certain sizes and shapes can pass through) and as traps for molecules so they can be analyzed. Zeolites are also widely used as adsorbents and catalysts. The zeolite is used as a molecular sieve to create purified oxygen from air using its ability to trap impurities, in a process involving the adsorption of nitrogen, leaving highly purified oxygen. Their well-defined pore structure and adjustable acidity make them highly active in a large variety of reactions. Synthetic zeolites are useful in petrochemical catalysis, for instance, in fluid catalytic cracking and hydrocracking. Zeolites confine molecules in small spaces, which cause changes in their structure

and reactivity. The hydrogen-form zeolites are powerful solid-state acids and can facilitate a host of acid-catalyzed reactions, such as isomerization, alkylation, and cracking. Zeolites have the potential of providing precise and specific separation of gases, including the removal of H_2O, CO_2, and SO_2 from low-grade natural gas streams. Other separations include noble gases, N_2, O_2, Freon, and formaldehyde.

1.3.4 Metal–Organic Frameworks

MOFs are compounds consisting of metal ions or clusters coordinated to organic ligands to form 1D, 2D, or 3D structures (Figure 1.5). They are a subclass of coordination polymers with the special feature of potential voids. In some cases, the pores are stable during elimination of the guest molecules (often solvents). The metal ions are typical di-, tri-, or tetravalent transition metals, and the ligands are usually organic carboxylic acid with multiple carboxyl groups that serve as the struts to connect metal ions or clusters, one example being 1,4-benzenedicarboxylic acid (H_2BDC).

To describe and organize the structures of MOFs, a system of nomenclature has been developed. Subunits of an MOF, called secondary building units (SBUs), can be described by topologies common to several structures. Each topology, also called a net, is assigned a symbol, consisting of three lowercase letters in bold. MOF-5, for example, has a **pcu** net. In addition to the topology structures, the chemistry of MOFs can be described using three descriptors: metal sites, organic ligands, and available pores. The choice of metal and linker dictates the structure and hence properties of the MOF. For example, the metal's coordination preference influences the size and shape of pores by dictating how many ligands can bind to the metal and in which orientation. Besides, the coordination modes between metal ions and linkers also allow the unsaturated metal sites and available groups on ligands for further functionalization. The spaces within MOF frameworks offer a large opportunity for host–guest chemistry, for instance, assembled nanopores can accommodate a huge amount of gases or liquids and provide pathways for molecular diffusion.

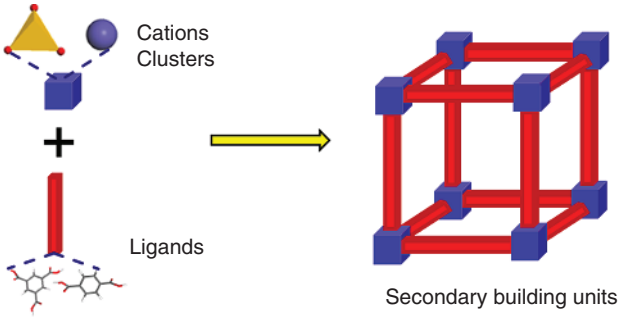

Figure 1.5 A scheme for the self-assembly of metal–organic frameworks by metal ions or clusters with organic linkers.

The syntheses of MOFs were developed from those of zeolites. MOFs are produced almost exclusively by hydrothermal or solvothermal techniques, where crystals are slowly grown from a hot solution. In contrast to zeolites, MOFs are constructed from bridging organic ligands that remain intact throughout the synthesis [113]. Zeolite synthesis often makes use of a template. Templates are ions that influence the structure of the growing inorganic framework. Typical templating ions are quaternary ammonium cations, which are removed later by calcination. In MOFs, the framework is templated by SBUs and organic ligands [114]. Post-synthetic modification of MOFs opens up possibilities that might not be achieved by conventional synthesis [115]. Of potential relevance to carbon dioxide capture are MOFs with amino groups. Such groups have been generated by post-synthetic grafting to the bridging ligands [116]. A solvent-free synthesis of a range of crystalline MOFs has been described [117]. Usually the metal acetate and the organic ligand are mixed and ground up with a ball mill. For example, $Cu_3(BTC)_2$ (named as HKUST-1) can be quickly synthesized in this way in quantitative yield.

The functions of MOFs offer them with a wide range of applications. MOFs attract attention as materials for adsorptive gas storage because of their high SSA and chemically tunable structures [118]. The most studied systems are hydrogen and methane storage. Compared with an empty gas cylinder, an MOF-filled gas cylinder can store more gas because of adsorption that takes place on the inner surface of MOFs. Furthermore, MOFs are free of dead volume, so there is almost no loss of storage capacity as a result of space blocking by non-accessible volume [119]. Also, MOFs have a fully reversible uptake-and-release behavior, since the storage mechanism is based primarily on physisorption. No large activation barriers are required when liberating the adsorbed hydrogen. In 2012, MOF-210 was predicted to have hydrogen storage capacity of 2.90 wt% (1–100 bar) at 298 K and 100 bar [120]. Another priority of MOFs applications is carbon capture and storage. Because of their small, tunable pore sizes and high void fractions, MOFs are a promising potential material for use as an adsorbent to capture CO_2. MOFs could provide a more efficient alternative to traditional amine solvent-based methods in CO_2 capture from coal-fired power plants [121]. MOFs could be employed in each of the main three carbon capture configurations for coal-fired power plants: pre-combustion, post-combustion, and oxy-combustion [122]. Since the post-combustion configuration is the only one that can be retrofitted to existing plants, it garners the most interest and research. In post-combustion carbon capture, the flue gas from the power plant would be fed through an MOF in a packed-bed reactor setup. Flue gas is generally 40–60 °C with a partial pressure of CO_2 at 0.13–0.16 bar. The main component CO_2 must be separated from is nitrogen, but there are small amounts of other gases as well. A typical flue gas composition is 73–77% N_2, 15–16% CO_2, 5–7% H_2O, 3–4% O_2, 800 ppm SO_2, 10 ppm SO_3, 500 ppm NO_x, 100 ppm HCl, 20 ppm CO, 10 ppm hydrocarbons, and 1.0 ppb Hg. MOF-177 exhibits a CO_2 capacity of 33.5 mmol g^{-1} at ambient temperature and 35 bar [123]. CO_2 can bind to the MOF surface through either physisorption or chemisorption, where physisorption occurs through van der Waals interactions and chemisorption occurs through covalent bonds being formed between CO_2 and MOF surface [124]. Once the MOF is saturated with CO_2, the MOF

would then be regenerated through either a temperature swing or a pressure swing process. Many potential uses of MOFs exist beyond adsorption or storage, such as gas purification/separation and heterogeneous catalysis. MOFs are promising for gas purification because of strong chemisorption that takes place between electron-rich molecules (such as amines, phosphines, alcohols, water, or sulfur-containing molecules) and the framework, allowing the desired gas to pass through the MOFs. Gas separation can be performed with MOFs because they can allow certain molecules to pass through their pores based on size and kinetic diameter. This is particularly important for separating out carbon dioxide. In principle, these same MOFs could also be used for catalysis because of their shape and size selectivity and their accessible bulk volume. Also, because of their very porous architecture, mass transport in the pores is not hindered. MOFs can be a substituent for the pervasive platform of zeolites, although MOF catalysts have not been commercialized. Their high surface area, tunable porosity, diversity in metal, and functional groups make them especially attractive in heterogeneous catalysis.

1.3.5 Highly Porous Polymers

1.3.5.1 High Free Volume Polymers

The main types of high free volume glassy polymers include substituted polyacetylenes, perfluoropolymers, poly(norbornene)s, polyimides (PIs), and thermally rearranged (TR) polymers. Chemical structures and molecular models of representative examples are shown in Figure 1.6. Regarding polymers having isolated double bonds in the main chain, poly(1,3-dienes) and polynorbornene are well known [125].

Natural rubber has a molecular weight up to around one million and cis-1,4-polyisoprene structure except two or three trans-1,4-units at the initiating chain end. Polynorbornene can be obtained by ring-opening metathesis polymerization (ROMP) of norbornene (NBE). ROMP is mediated by metal carbenes such as Schrock's molybdenum carbenes and Grubbs Ru

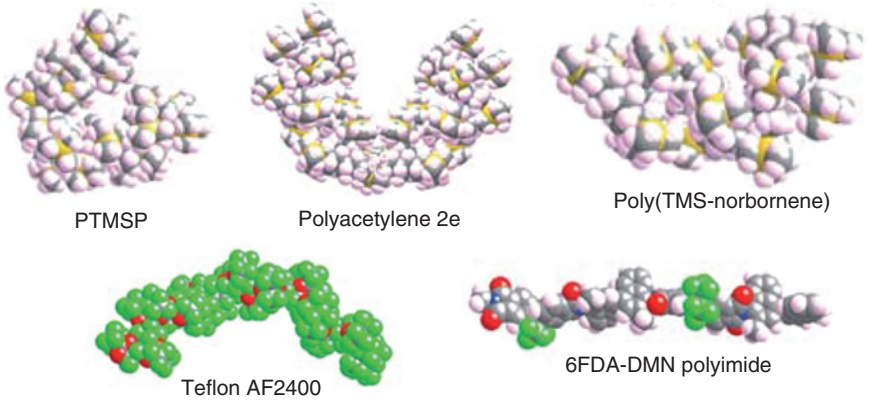

Figure 1.6 Molecular models of representative porous polymers.

carbenes [126]. Polymerization of acetylene and its analogues, which provides polymers having conjugated carbon–carbon double bonds, has also been studied considerably. The presence of carbon–carbon alternating double bonds in the main chain of substituted polyacetylenes and poly(norbornene)s endows them with unique properties such as conductivity, nonlinear optical properties, magnetic properties, gas permeability, photoluminescent and electroluminescent properties, and so on. The most famous function of substituted polyacetylenes and poly(norbornene)s is gas separation membrane. In particular, poly[(1-trimethylsilyl)-1-propyne] [poly(11)] is famous because it shows the highest gas permeability among all the existing polymers, and hence its gas permeability has been extensively studied so far [127]. Addition-type poly(trimethylsilyl norbornene), prepared with nickel naphthenate as catalyst and methylaluminoxane as co-catalyst, exhibited high free volume and high permeability [128]. Perfluoropolymers are fluorocarbon-based polymers with multiple carbon–fluorine bonds. It is characterized by a high resistance to solvents, acids, and bases. This unique class of polymers has been widely used in membrane technology for their excellent chemical and thermal stability, high mechanical strength, and versatile processability. The main application areas of fluoropolymer membranes have been focused on MF, UF, and battery separators [129]. Recently, however, the application ranges are expanding into new innovative applications like MBR, membrane distillation (MD), membrane crystallization (MCr), and PV. Also, some soluble perfluoropolymers are capable to form amorphous glassy films with specific application in gas separation. The most studied ones are Teflon AF2400 and Teflon AF1600, which are copolymers of 2,2-bistrifluoromethyl-4,5-difluoro-1,3-dioxole and tetrafluoroethylene with mole fractions of the dioxole of 0.87 and 0.65, respectively [130].

PI is a polymer of imide monomers. Several methods are possible to prepare PIs, including the reaction between a dianhydride and a diamine and the reaction between a dianhydride and a diisocyanate [131]. According to the type of interactions between the main chains, PIs can be classified into thermoplastic and thermosetting PIs. Thermosetting PIs are known for thermal stability, good chemical resistance, excellent mechanical properties, and characteristic orange/yellow color. Most PIs are not affected by commonly used solvents and oils including hydrocarbons, esters, ethers, alcohols, and freons. With their high heat resistance, PIs enjoy diverse applications in roles demanding rugged organic materials, e.g. high temperature fuel cells, displays, and various military roles. Some PIs, such as CP1, are solvent soluble and exhibit high optical clarity. The solubility properties lend them toward spray and low temperature cure applications. These PIs can be processed into membranes for reverse osmotic purification of water or filters for separating dust and particulate matter from the exhaust gas. Significant development of some PI membranes is witnessed in gas separation owing to the creation of large porosity in the membranes in recent years. They are commonly prepared by a step polymerization involving a cycloimidization reaction between a bis(carboxylic anhydride) and a diamine. Many PIs exhibit good selectivity, but at the expense of modest permeability. A few, however, show high permeability, in particular those prepared from

4,4′-(hexafluoroisopropylidene)diphthalic anhydride (6FDA) with diamines such as 2,3,5,6-tetramethyl-1,4-phenylenediamine (4MPDA) [132].

Many other polymer structures can be envisaged that would exhibit desirable membrane properties, but which cannot be prepared in soluble form. An alternative route to high free volume membranes is to use a soluble precursor to prepare the membrane and subsequently to generate the desired structure by thermal treatment. Park et al. demonstrated this approach using soluble aromatic PIs with −OH or −SH groups in the *ortho* position, which rearrange irreversibly to insoluble, infusible polybenzoxazoles or polybenzothiazoles on heating at temperatures of 350–450 °C [133]. These TR polymers exhibited gas separation performances in CO_2/CH_4 gas pair.

1.3.5.2 Porous Organic Frameworks

Recently, POFs are emerging as a new class of microporous materials. POFs are composed of organic moieties connected by strong covalent bonds, resulting in ordered and rigid structures (Figure 1.7).

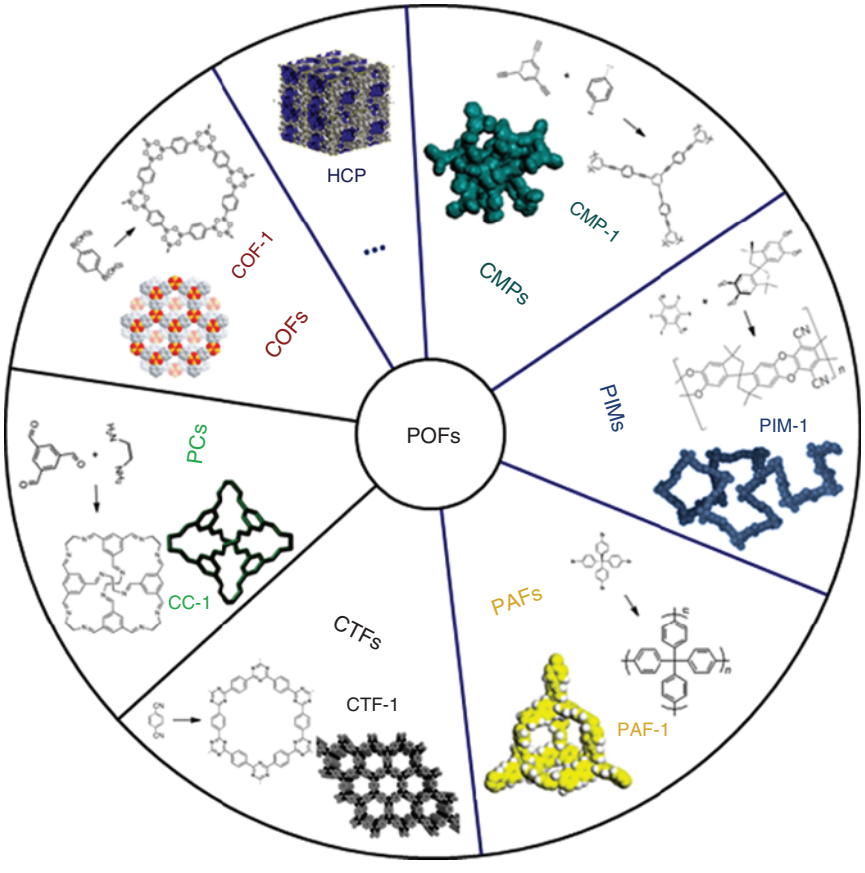

Figure 1.7 Chemical structures of different catalogues of porous organic frameworks (POFs).

POFs can be mainly categorized into the following subclass materials: polymers of intrinsic microporosity (PIMs), covalent organic frameworks (COFs), conjugated microporous polymers (CMPs), covalent triazine-based frameworks (CTFs), hypercrosslinked polymers (HCPs), porous cages (PCs), porous aromatic frameworks (PAFs), etc. [134]. Typically, crystalline COFs and PCs are created by reversible reactions through forming boroxine, imine, or hydrazone units. In 2005, Yaghi et al. firstly reported the successful synthesis of two COFs (COF-1, COF-5) by condensation reactions of phenyldiboronic acid of $C_6H_4[B(OH)_2]_2$ and hexahydroxytriphenylene of $C_{18}H_6(OH)_6$ [135]. The two compounds were crystalline products with 2D expanded porous graphitic layers. Their crystal structures are entirely held by strong bonds between B, C, and O atoms to form rigid porous architectures with pore sizes ranging from 0.7 to 2.7 nm. The synthesis of 3D COFs has been hindered by long-standing practical and conceptual challenges. Unlike 0D and 1D system, the insolubility of 2D and 3D structures precludes the use of stepwise synthesis, making their isolation in crystalline form very difficult. The first challenge, however, was overcome by judiciously choosing building blocks and using reversible condensation reactions to crystallize COFs. Examples of 3D COFs are COF-102, COF-103, COF-105, COF-108, COF-202, and COF-300. Most of 3D COF show high surface area, which surpass those of 2D (3472, 4210, and 3214 $m^2\ g^{-1}$ for COF-102, COF-103, and COF-202 respectively) [136]. COFs can be synthesized by either boron or imine condensation. The most popular COF synthesis route is a boron condensation reaction that is a molecular dehydration reaction between boronic acids. In the case of COF-1, three boronic acid molecules converge to form a planar six-membered B_3O_3 (boroxine) ring with the elimination of three water molecules. A new class of COFs can be obtained by imine condensation of aniline with benzaldehyde that results in imine bond formation with elimination of water. COF-300 is a good example of this chemistry [137]. The main applications of COFs can be divided into two directions: gas storage and optical devices. Yaghi et al. reported several COFs as exceptional hydrogen and methane storage materials. Highly conjugated and layered COFs are promising in making optical devices. For instance, a highly ordered π-conjugation TP-COF, consisting of pyrene and triphenylene functionalities alternately linked in a mesoporous hexagonal skeleton, is highly luminescent, harvests a wide wavelength range of photons, and allows energy transfer and migration [138].

CTFs are also crystalline or semicrystalline triazine-based materials, produced by ionothermal syntheses. The development of CTFs formed by trimerization of aromatic nitriles in molten $ZnCl_2$ was first reported by Thomas and colleagues [139]. These CTFs possess very high surface areas (up to 3300 $m^2\ g^{-1}$), large pore size (up to 4.3 nm), and high amounts of nitrogen functionalities in the networks. Because of the fully covalent structure and the rigid aromatic network, CTF polymers possess very high thermal and chemical stability, making them attractive candidates as new catalyst supports. The development of a CTF (CTF-6) loaded with platinum salts and its use as a catalyst for methane oxidation were reported by Palkovits et al. [140]. The catalysts exhibit extraordinary stability under harsh reaction conditions of concentrated sulfuric acid at 215 °C. CTFs have recently

emerged as a versatile platform for the deployment of catalysts, such as asymmetric catalysis and heterogeneous organic catalysis [141].

PIMs contain highly rigid main chains and bulky side substituents that prevent efficient chain packing, leading to high porosities. A program of research commenced in Manchester aimed at generating organic microporous materials through step-growth polymerization. The initial objective was to link the polymer network through rigid, nonlinear linking units that would inhibit co-facial association and prevent structural relaxation. A suitable linking unit is derived from the commercially available monomer 5,5′,6,6′-tetrahydroxy-3,3,3′,3′-tetramethyl-1,1′-spirobisindane. The fused ring structure gives rigidity and the spirocenter (i.e. a single tetrahedral carbon atom shared by two rings) makes it nonlinear (i.e. provides a site of contortion). A double aromatic nucleophilic substitution reaction with 4,5-dichlorophthalonitrile yields a bis(phthalonitrile) precursor that forms a phthalocyanine network via a cyclotetramerization facilitated by a metal ion template [142]. The network polymers are obtained as highly colored, free-flowing insoluble powders. Due to the efficient prevention of macromolecule backbone, the PIMs showed high apparent surface areas (500–1000 $m^2\ g^{-1}$). The next objective was to establish a more general route to microporous network polymers. The remarkably efficient double aromatic nucleophilic substitution (i.e. dioxane-forming reaction) [143] between an aromatic monomer bearing multiple hydroxyl groups and an aromatic monomer bearing multiple fluorines (or chlorines) proved eminently suitable. To obtain an intrinsically microporous polymer, at least one of the monomers must contain a site of contortion such as a spirocenter, a nonplanar rigid skeleton, or a single covalent bond about which rotation is severely hindered. For network formation, the average functionality of the pair of monomers should be greater than 2, with each pair of adjacent hydroxyl groups or fluorines counting as a single functional group for dioxane formation. Having established a general approach to microporous networks, the potential of non-network polymers formed from pairs of bifunctional monomers was explored [144]. The polymer of PIM-1 is soluble in solvents such as tetrahydrofuran and chloroform and can be precipitated as a powder or cast from solution to form a robust membrane. PIM-1 in powder or membrane form has a high apparent surface area and exhibits microporous character. The common features of a PIM are (i) no or very highly restricted rotational freedom about all bonds in the backbone and (ii) the inclusion of sites of contortion such as spirocenters. Due to the intrinsic microporosity and membrane-formation ability, PIMs were explored for membrane application [145]. Membranes of PIM-1 were tested for the removal of organic compounds from aqueous solution by PV [144]. The membranes are organophilic, the permeate being enriched in the organic component (e.g. a feed of 5 wt% phenol in water gave a permeate of nearly 50 wt% phenol), and the fluxes achieved were comparable to the rubbery polymer poly(dimethylsiloxane).

PAFs are extraordinarily high-surface-area and permanently porous materials, which are usually synthesized by forming strong C—C bonds between aromatic monomers through coupling reactions. The original idea for the synthesis of PAF-1 can be dated back to 2009. Inspired by the structure and properties of diamond, C—C covalent bond of diamond was replaced by rigid phenyl rings

with the same tetrahedron configuration. This insertion allows sufficient exposure of the faces and edges of phenyl rings with the expectation of increasing the internal surface areas. Followed by the molecular design, tetraphenylmethane building blocks and the Yamamoto-type Ullmann cross-coupling reaction were employed for constructing PAF with *dia* topology (PAF-1) [146]. Structure characterization revealed that PAF-1 had a record surface area ($S_{BET} = 5640\ m^2\ g^{-1}$) at that time and exceptional physicochemical stability with permanent porosity against thermal and chemical etching. Further, a series of PAFs were synthesized by the same topology chemistry and suitable coupling reactions, which were exemplified by PAF-3 and PAF-4 with Si and Ge centers [147]. In order to achieve the high surface areas, complementary cross-coupling reactions such as Sonogashira–Hagihara routes and Suzuki cross-coupling were adopted for creating a sheer number of PAF materials (PAF-1 to PAF-76) [148]. Owing to the extremely high porosity, PAFs were widely used in gas adsorption and storage. For example, high-pressure hydrogen storage of PAF-1, PAF-3, and PAF-4 was determined at 77 K, and the excess hydrogen uptake capacity is 7.0 wt% at 48 bar, 5.5 wt% at 60 bar, and 4.2 wt% at 60 bar for PAF-1, PAF-3, and PAF-4, respectively [146–148]. Based on the aromatic nature, PAFs are promising in oil cleanup by adsorbing organics from water [149]. Other potential applications in electrochemical devices and catalysis are being developed [150].

CMPs are another type of high-surface-area POFs, which are generally prepared by linking ethynyl derivatives and second halogen monomers into amorphous and extended networks. To generate the porous structure of CMPs, cross-coupling of building blocks with different geometries to create a 3D polymer backbone is necessary, while self-condensation reactions occur in the homocoupling of building blocks with similar geometry [134]. Several physical properties of CMPs can be attributed to their extended conjugation or microporosity. Much like conductive metals, conjugated polymers exhibit electronic bands. The electrons of the conjugated system occupy the valence band, and removal of electrons from this band or addition of electrons to the higher-energy conductive band can lead to conductivity [151]. Conjugated materials can in many cases absorb visible light because of their delocalized π-system. These properties have led to applications in organic electronics and organic photonics [152]. By taking advantage of both their electronic properties and porous nature, several CMPs have been applied in photovoltaics by incorporating inorganic materials (TiO_2) in pores and the electron-conducting skeletons [153]. A main drawback of CMPs is their inherent insolubility. This insolubility is caused by the long rigid moieties of the monomers. Several efforts have been made to increase solubility by the addition of solubilizing side chains, but this still remains a barrier to broad applications. In summary, the majority of POF materials possess high surface areas, exceptionally high thermal stability (up to 600 °C), tunable pore size, low framework density, and multifunctionality. The good physicochemical properties endow POFs with potential applications in gas sorption and storage, catalysis, opt-electric devices, and biomedical systems. Thus, intensive effort has been attracted on the synthesis and characterization of POFs with diversified chemical structures as well as on expanding the research scope to interdisciplinary areas including new directions of advanced applications.

1.4 Fundamentals of Membrane Separation

1.4.1 Membrane Definition

The membrane can be defined essentially as a barrier that separates two phases and restricts transport of various chemicals in a selective manner (Figure 1.8). A membrane can be homogeneous or heterogeneous, symmetric or asymmetric in structure, or solid or liquid, can carry a positive or negative charge, or can be neutral or bipolar. Transport through a membrane can be affected by convection or by diffusion of individual molecules, induced by an electric field or concentration, pressure, or temperature gradient. The membrane thickness may vary from as small as several nanometers to millimeters.

A membrane separation system separates an influent upstream into two effluent downstreams known as permeate and concentrate. Permeate is the portion of the fluid that has passed through the semipermeable membrane, whereas the concentrate stream contains the constituents that have been rejected by the membrane. Membrane separation process enjoys numerous industrial applications with the following advantages: appreciable energy savings; environmentally benign; clean technology with operational ease; the potentiality to replace the conventional processes like filtration, distillation, ion exchange, and chemical treatment systems; the possibility to produce high-quality products; greater flexibility in designing systems; etc. The proper choice of a membrane should be determined by the specific application objective: particulate or dissolved solids removal, hardness reduction or ultrapure water production, removal of specific gases/chemicals, etc. The end use may also dictate selection of membranes for industries such as portable water, effluent treatment, desalination, or water supply for electronics or pharmaceutical manufacturing.

1.4.2 Transport Theory

Theories of membrane transport phenomena for both gas and liquid separations have been described.

1.4.2.1 Membrane Transport for Gas Systems

There are two main membrane permeation mechanisms: (i) through dense membranes and (ii) through porous membranes.

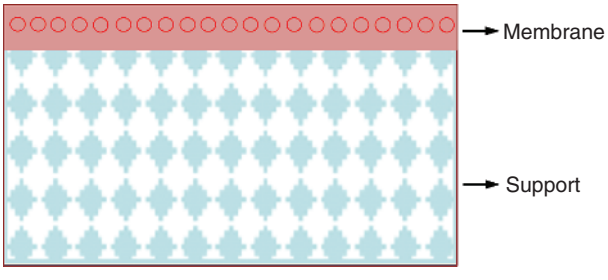

Figure 1.8 Schematic representation of a supported membrane.

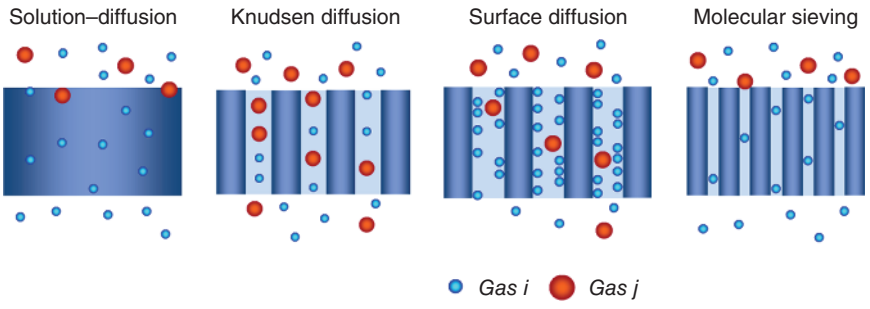

Figure 1.9 Gas transport mechanisms in membranes.

1. The solution–diffusion mechanism is the commonly used physical model to describe gas transport through dense membranes. A schematic picture is provided in Figure 1.9 for better illustration. A gas molecule is adsorbed on one side of the membrane, dissolves in the membrane material, diffuses through the membrane, and desorbs on the other side of the membrane. If diffusion through the membrane takes place in the form of ions and electrons (i.e. proton-exchange transport) or as atoms (e.g. for hydrogen transport through dense metal), the molecule needs to split up after adsorption and recombine after diffusing through the membrane.
2. As displayed in Figure 1.9, three types of transport mechanisms are proposed with respect to separation in porous membranes: Knudsen diffusion, surface diffusion, and molecular sieving [154]. In some cases, molecules can move through the membrane by more than one mechanism. Knudsen diffusion gives relatively low separation selectivity compared with surface diffusion. Molecular sieving can yield high selectivity due to shape-selective separation. The separation factor for these mechanisms depends on pore size distribution, temperature, pressure, and interactions between gases being separated and the membrane surfaces. Knudsen (or free-molecule) diffusion takes place for the cases with a large Knudsen number (K_n), which is defined as the ratio of the mean free path of the gas molecules (average distance between collisions) and a representative physical length scale (e.g. the pore radius). If the pore radius is used as representative physical length scale, the mean free path lengths are substantially higher than pore radii at $K_n > 10$, which results in the lighter molecules permeating through the pores. In this case, selectivity is limited and can be calculated with the square root of the ratio of the molar masses of the gases involved. The smaller the Knudsen number, the larger the pores become (relative to the mean free path of the gas molecules), and the lower selectivity becomes. For $K_n < 1.0$, the dominant transport mechanism is viscous flow, which is nonselective.

Surface diffusion may occur in parallel with Knudsen diffusion. Gas molecules are adsorbed on the pore walls of the membrane and migrate along the surface. Surface diffusion increases the permeability of the components adsorbing strongly to the membrane pores. At the same time, the effective pore diameter is

reduced. Consequently, transport of non-adsorbing components is reduced and selectivity is increased. This positive contribution of surface diffusion works for certain temperature ranges and pore diameters. If pore sizes become sufficiently small (3–5 Å), the mechanism of molecular sieving is applicable in separating molecules that differ in kinetic diameter. The pore size becomes so small that only the smaller gas molecules can permeate through the membrane.

1.4.2.2 Membrane Transport for Liquid Systems

In membrane filtration, the separation process is accomplished by using a differential driving potential across a membrane having selective permeability. For example, the differential driving potential used to transport solvent across UF membrane is the hydrostatic pressure. UF is commonly used to separate suspended solids, colloids, and macromolecules from water. Whenever the solvent of a mixture flows through the membrane, retained species are locally concentrated at the membrane surface, thereby resisting the flow. This localized concentration of solute normally results in precipitation of a solute gel over the membrane. Hence, UF throughput depends on physical properties of the membrane, such as permeability, thickness, and process/system variables such as feed concentration, system pressure, velocity, and temperature. Two models of gel polarization and resistance with different approaches are described below.

Gel Polarization Model The basic assumptions of this model are as follows:

1. UF membranes have skin that offers minimum resistance to flow, and the asymmetry of the pore virtually eliminates internal pore fouling.
2. Concentration buildup at the membrane surface rises up to the point of incipient gel precipitation, forming a dynamic secondary membrane on top of the primary structure.
3. The secondary membrane offers the major resistance to flow.
4. The gel layer grows in thickness until the pressure-activated convective transport of solute with solvent toward the membrane surface just equals the concentration gradient-activated diffusive transport away from the membrane surface.
5. Beyond a certain threshold pressure, increase in pressure does not improve the flux because the gel layer grows thicker to offer more resistance to the increased driving force. This is called critical flux:

$$J_w = \frac{P}{R_c + R_m}$$

   where
   J_w is the water flux
   P is the transmembrane pressure
   R_c is the resistance of the deposited cake
   R_m is the hydraulic resistance of the membrane
6. Eventually, the concentration at the membrane surface will be high enough to form a gel.

7. In the steady state, the convective transport to the membrane must equal the back-diffusive transport away from the membrane:

$$J = -D\left(\frac{d_c}{d_x}\right)$$

where
J is the solvent flux through the membrane
C is the concentration of solutes or colloids retained in membrane
D is the solute diffusivity
x is the distance from the membrane surface
By *integration*, it gives

$$J = \left(\frac{D}{\delta}\right) \cdot \ln\left(\frac{C_g}{C_b}\right) = k \cdot \ln\left(\frac{C_g}{C_b}\right)$$

where
k is the mass transfer coefficient
δ is the *boundary* layer thickness considering D as constant
C_g and C_b represent the maximum solute concentration in the gel layer and the concentration of solutes in the bulk of the feed, respectively

8. Lower solute concentration (C_b) will have higher threshold pressure because much higher flux is required to transport enough solute to the membrane to begin to form a gel.

Resistance Model The mechanism of separation in UF involves not only the size exclusion but also the adsorption and surface charge characteristics of membranes. In the absence of a solute, the water flux through a microporous membrane is defined by Darcy's law, which states that pure solvent flux is directly proportional to the applied pressure differential (ΔP) and inversely proportional to pure solvent viscosity (μ_w):

$$J_w = \frac{\Delta P}{R_m \mu_w}$$

where R_m is the membrane hydraulic resistance, which is a function of pore size, tortuosity, membrane thickness, and porosity.

If the feed solution contains solutes that are retained at the membrane interface, the water flux in UF is generally lower than pure water flux. A number of phenomena have been suggested to account for this flux reduction, such as resistance due to gel layer formation, resistance due to concentration polarization, and resistance due to an absorption layer and pore plugging. For a macromolecular solute of high molecular weight at low concentration, the osmotic pressure effect can be neglected. The effect of the gel layer can be represented as

$$J_{uf} = \frac{\Delta P_{appl}}{\mu_w (R_m + R_p)}$$

where R_p is the resistance due to gel polarization.

The time-dependent case of above equation can be represented as

$$J_{uf}(t) = \frac{\Delta P_{appl}}{\mu_w[R_m + R_p(t)]}$$

After testing, if the membrane is thoroughly washed with appropriate washing solution and the pure water flux (J_w) is determined at the same ΔP, it may be found to be less than J_w but still greater than J_{uf}. The difference between J_w and J_{uf} may be accounted for by the irreversible fouling due to adsorption of solute on the membrane, and this loss in flux can be visualized as additional resistance to the flux (R_a):

$$J_w = \frac{\Delta P_{appl}}{\mu_w(R_m + R_a)}$$

Hence, incorporating R_a, above equation can be written as

$$J_{uf}(t) = \frac{\Delta P_{appl}}{\mu_w[R_m + R_a + R_p(t)]}$$

It is noted that J_{uf} reaches an almost constant final flux $J_{uf}(F)$ and the time corresponding to this $J_{uf}(F)$ is $t(F)$. At this stage, $R_p(t)$ becomes constant $R_p(F)$:

$$J_{uf}(F) = \frac{\Delta P_{appl}}{\mu_w[R_m + R_a + R_p(F)]}$$

There also exists a concentration polarization resulting from the relative rate of solute transport to the membrane surface by convection and the back-diffusive solute flux. Although both concentration polarization and fouling reduce the membrane flux, they have opposing effects on the observed percent rejection. Another way to distinguish the two phenomena is through their time dependence. Concentration polarization is dependent on operating parameters such as pressure, temperature, feed concentration, and velocity but is not a function of time. Fouling is partially dependent on these variables, particularly feed concentration, but is also a function of time.

The change of flux with time due to different kinds of resistances is given in Figure 1.10 for a typical UF membrane [155]. It shows asymptotic behavior after a particular duration of time.

The mass transfer coefficient, k, can be calculated from the following equation:

$$k = \frac{PR}{3600 M_B S \left[\frac{1+m(1-f)M_A}{1000}\right] c(1 - X_3)\left[\ln\left(\frac{X_2 - X_3}{X_1 - X_3}\right)\right]}$$

where

PR refers to the product rate
f refers to the solute separation with reference to the chosen reference solute
M_A and M_B refer to the molecular weights of solute and water, respectively
S refers to the membrane area
m is the solute molarity
c is the molar density of feed

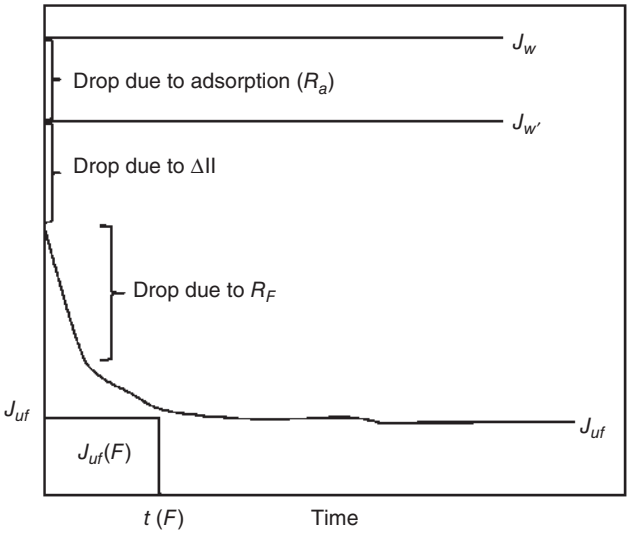

Figure 1.10 Change of flux with time for UF membrane showing asymptotic behavior after a particular duration of time.

X_1, X_2, and X_3 refer to the mole fractions of solute at bulk, membrane–solution interface, and membrane-permeated product, respectively

1.4.2.3 Transport Mechanism in ED Membrane

The transport mechanism in the ED membrane is shown in Figure 1.11, showing concentration and potential gradients in a well-stirred ED cell. In this example, chloride ions easily permeate the anionic membranes containing fixed positive groups and are stopped by the cationic membranes containing fixed negative groups. Similarly, sodium ions permeate the cationic membranes but are stopped by the anionic membranes. The overall result is increased salt concentration in

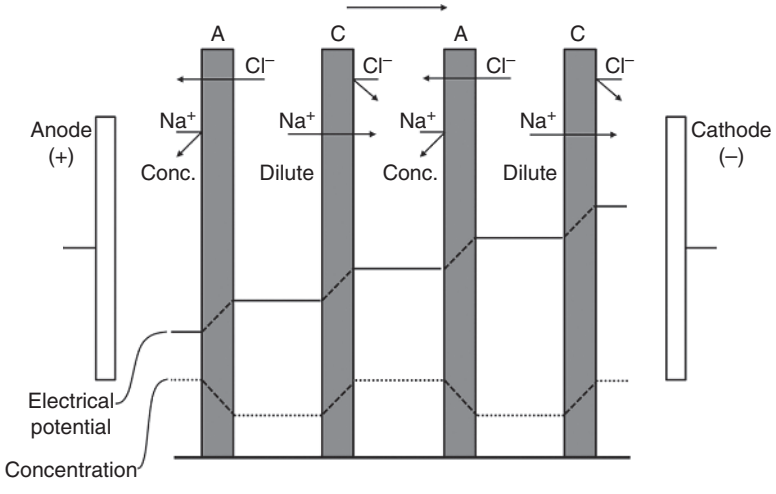

Figure 1.11 Schematic of concentration and potential gradients in a well-stirred ED cell.

alternating compartments, whereas the other compartments are simultaneously depleted of salt. The voltage potential drop caused by the electrical resistance takes place entirely across the ion-exchange membrane. In a well-stirred cell, the flux of ions across the membranes and hence the productivity of the ED system can be increased without limit by increasing the current across the stack. In practice, however, the resistance of the membrane is often small in proportion to the resistance of the water-filled compartments, particularly in the dilute compartment where the concentration of ions carrying the current is low. In this compartment, the formation of ion-depleted regions next to the membrane places an additional limit on the current and hence the flux of ions through the membranes. Ion transport through this ion-depleted aqueous boundary layer generally controls ED system performance.

The formation of concentration gradients caused by the flow of ions through a cationic membrane is shown in Figure 1.12. It shows the concentration gradient of univalent sodium ion next to a cationic membrane. Exactly equivalent gradient of anion, such as chloride ion, forms adjacent to the anionic membranes in the stack. The ion gradient formed on the left dilute side of the membrane can be described by Fick's law.

Thus, the rate of diffusion of cations to the surface is given by

$$J^+ = \frac{D^+(c^+ - c^+_{(0)})}{\delta}$$

where

D^+ is the diffusion coefficient of the cation in water
c^+ is the bulk concentration of the cation in the solution
$c^+_{(0)}$ is the concentration of the cation in the solution adjacent to the membrane surface (0)
δ is film thickness

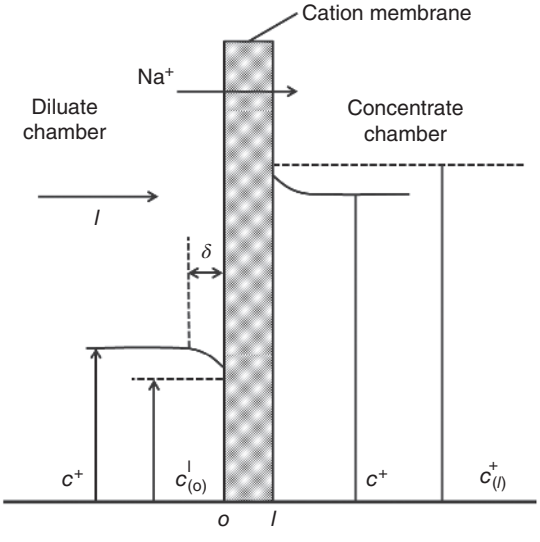

Figure 1.12 Schematic of concentration gradients adjacent to a single cationic membrane in an ED stack.

The rate at which the cations approach the membrane by electrolyte transport is (t^+I/F). The total flux of sodium ions to the membrane surface (J^+) is the sum of these two terms:

$$J^+ = \frac{D^+(c^+ - c^+_{(0)})}{\delta} + \left(\frac{t^+ I}{F}\right)$$

Transport through the membrane is also the sum of two terms (i) due to the voltage difference and (ii) due to the diffusion caused by the difference in ion concentrations on each side of the membrane. Thus, the ion flux through the membrane can be written as

$$J^+ = \left(\frac{t^+_{(m)} I}{F}\right) + \frac{P^+(c^+_{(0)} - c^+_{(1)})}{1}$$

where P^+ is the permeability of the sodium ions in a membrane of thickness l.

The quantity $P^+(c^+_{(0)} - c^+_{(1)})/l$ is much smaller than transport due to the voltage gradient, so above two equations can be combined and simplified to

$$\left(\frac{t^+ I}{F}\right) + \frac{D^+(c^+ - c^+_{(0)})}{\delta} = \left(\frac{t^+_{(m)} I}{F}\right)$$

For a selective cationic ion-exchange membrane for which $t^+_{(m)} = 1$, it can be further simplified to

$$I = \left(\frac{FD^+}{1 - t^+}\right) \frac{(c^+ - c^+_{(0)})}{\delta}$$

This important equation has a limiting value when the concentration of the ion at the membrane surface is zero ($c^+_{(0)} = 0$). At this point, the current reaches its maximum value. The limiting current is given by the equation

$$I_{\text{lim}} = \frac{FD^+ c^+}{\delta(1 - t^+)}$$

The limiting current, I_{lim}, is the maximum current that can be employed in an ED process. If the potential required to produce this current is exceeded, the extra current will be carried by other processes, first by transport of anions through the cationic membrane and, at higher potentials, by hydrogen and hydroxyl ions formed by dissociation of water. Both of these undesirable processes consume power without producing any separation. This decreases the current efficiency of the process.

The limiting current density for an ED system operated at the same feed solution flow rate is a function of the feed solution salt concentration. As the salt concentration in the solution increases, more ions are available to transport current in the boundary layer, so the limiting current density also increases. For this reason, large ED systems with several ED stacks in series will operate with different current densities in each stack, reflecting the change in the feedwater concentration as salt is removed.

1.5 Membrane Configurations

As discussed above, membrane materials with the appropriate chemical, mechanical, and permeation properties are crucial for high-performance membranes. In addition, the technology contributes greatly in successfully fabricating this material into a robust, thin, defect-free membrane and then to package the membrane into an efficient, economical, high-surface-area module. This chapter covers the membrane structures, preparation techniques, technology, and modules.

1.5.1 Membrane Structures

As shown in Figure 1.13, membrane structures are organized in a sequence of microporous membranes, homogeneous membranes, asymmetric membranes, electrically charged membranes, and liquid membranes.

1. Microporous membranes: The membrane behaves almost like a fiber filter and separates by a sieving mechanism determined by the pore diameter and particle size. Materials such as inorganics or organics are used in making such membranes. The pores in the membrane may vary between 0.3 nm and 100 μm.
2. Homogeneous membranes: This is a dense film through which a mixture of molecules is transported by pressure, concentration, or electrical potential gradient. Using these membranes, chemical species of similar size and diffusivity can be separated efficiently when their concentrations differ significantly.
3. Asymmetric membranes: An asymmetric membrane comprises a very thin (0.1–1.0 μm) skin layer on a highly porous (50–500 μm) thick substructure.

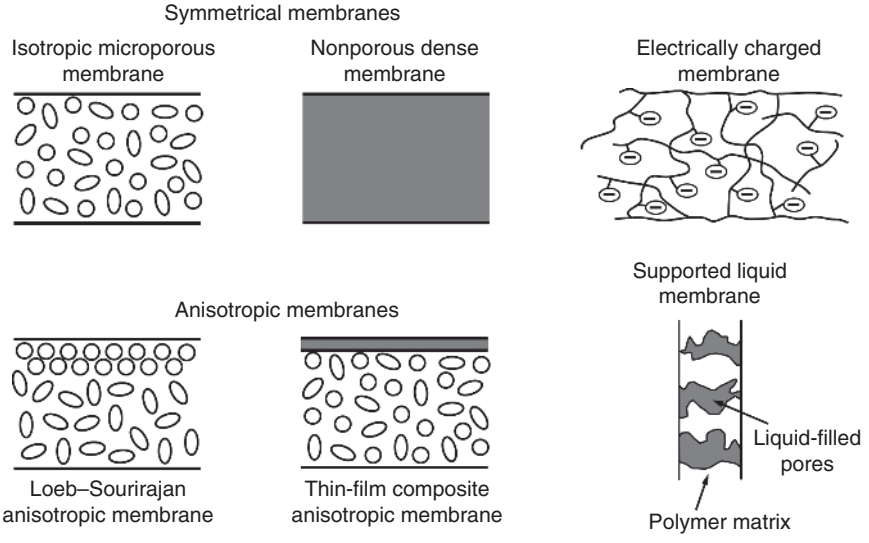

Figure 1.13 Schematic diagrams of the commonly used membranes.

The thin skin acts as the selective membrane. Its separation characteristics are determined by the nature of membrane material or pores size, and the mass transport rate is determined mainly by the skin thickness. Porous sublayer acts as a support for the thin, fragile skin and has little effect on the separation characteristics.

4. Electrically charged membranes: These are necessarily ion-exchange membranes consisting of highly swollen gels carrying fixed positive or negative charges. These are mainly used in the ED.
5. Liquid membranes: A liquid membrane utilizes a carrier to selectively transport components such as metal ions at relatively high rate across the membrane interface.

1.5.2 Preparation Techniques

Large-scale and industrial processes for preparing membranes can be mainly catalogued as (i) solution casting, (ii) melt extrusion, (iii) spinning, (iv) spin coating, (v) slip coating sintering, (vi) sol–gel technique, and (vii) carbonization.

1.5.2.1 Solution Casting

Solution casting is often used to prepare small samples of membrane for laboratory characterization experiments. An even film of an appropriate solution suspension is spread across a flat plate with a casting knife. The casting knife consists of a steel blade, resting on two runners, arranged to form a precise gap between the blade and the plate onto which the film is cast. After casting, the solution is left to stand, and the solvent evaporates to leave a thin and uniform film [156]. Appropriate solution viscosity and solvent type are required for preparing high-quality membranes or films. The solution used for solution casting should be sufficiently viscous to prevent it from running over the casting plate, so typical concentrations are in the range of 15–20 wt%. Preferred solvents are moderately volatile liquids such as acetone, ethyl acetate, and cyclohexane. Films cast from these solutions are dry within a few hours. When the solvent has completely evaporated, the dry film can be lifted from the glass plate. If the film adheres to the plate, soaking in a swelling non-solvent such as water or alcohol will usually loosen the film.

1.5.2.2 Melt Extrusion

Many polymers or inorganic polymer hybrids, including polyethylene, polypropylene, nylons, and silica gel, do not dissolve in appropriate solvents at room temperature, so membranes cannot be made by solution casting. The polymer is compressed between two heated plates. Typically, a pressure of 2000–5000 psi is applied for one to five minutes, at a plate temperature just below the melting point of the polymer or the matrix in the hybrid. Melt extrusion is also used on a very large scale to make dense films for packaging applications, either by extrusion as a sheet from a die or as blown film [157].

1.5.2.3 Spinning

Spinning is a manufacturing process for creating fiber membranes [158]. It is a specialized form of extrusion that uses a spinneret to form multiple continuous filaments. There are many types of spinning: wet, dry, dry jet-wet, melt, gel, and electrospinning. First, the precursor usually a polymer being spun must be converted into a fluid state. The fluid can be achieved from melting or dissolution in a solvent. For melted fluid, it is forced through the spinneret, and then it cools to a rubbery state and then a solidified state. For hot solution, the solvent is removed after being forced through the spinneret.

1.5.2.4 Spin Coating

Spin coating is widely used in the electronics industry to coat photoresists and photolithographic films onto silicon wafers [159]. The technique is also used in the laboratory to make composite membranes of 0.5–10 μm thick. An excess of dilute solution is placed on the substrate, which is then rotated at high speed. Fluid spins off the edge of the rotating substrate until the desired film thickness is achieved. The coating layer thickness can be decreased by increasing the rotation speed or decreasing the concentration in the applied solution.

1.5.2.5 Slip Coating Sintering

Slip-coating-sintering procedure was widely adopted for producing inorganic membranes, particularly for ceramic membranes with pore diameters in MF and UF range from 0.01 to 10 μm. In the slip-coating-sintering process, a porous ceramic support tube is made by pouring a dispersion of a fine-grain ceramic material and a binder into a mold and sintering at high temperature. The pores between the particles that make up this support tube are large. One surface of the tube is then coated with a suspension of finer particles in a solution of a cellulosic polymer or poly(vinyl alcohol), which acts as a binder and viscosity enhancer to hold the particles in suspension. This mixture is called a slip suspension; when dried and sintered at high temperatures, a finely microporous surface layer remains. Usually several slip-coated layers are applied in series, each layer being formed from a suspension of progressively finer particles and resulting in an anisotropic structure. Most commercial ceramic UF membranes are made this way, generally in the form of tubes or perforated blocks [160].

1.5.2.6 Sol–Gel Technique

Sol–gel method is used to produce membranes with pores from 10 to 100 Å. In this process, slip coating is taken to the colloidal level. Generally, the substrate to be coated with the sol–gel is a microporous ceramic tube formed by the slip-coating-sintering technique. This support is then solution coated with a colloidal or polymeric gel of an inorganic hydroxide. These solutions are prepared by controlled hydrolysis of metal salts or metal alkoxides to hydroxides. Sol–gel methods fall into two categories, depending on how the colloidal coating solution is formed [161]. In the particulate-sol method, a metal alkoxide dissolved in alcohol is hydrolyzed by addition of excess water or acid. The precipitate that results is maintained as a hot solution for an extended period during which the precipitate forms a stable colloidal solution. This process is called peptization. The

colloidal solution is then cooled and coated onto the microporous support membrane. The layer formed must be dried carefully to avoid cracking the coating. In the final step the film is sintered at 500–800 °C. In the polymeric sol–gel process, partial hydrolysis of a metal alkoxide dissolved in alcohol is accomplished by adding the minimum of water to the solution. The active hydroxyl groups on the alkoxides then react to form an inorganic polymer molecule that can then be coated onto the ceramic support. On drying and sintering, the inorganic film forms. Depending on the starting material and the coating procedure, a wide range of membranes can be made by the sol–gel process.

1.5.2.7 Carbonization

Carbonization is a particular method for producing carbon-based membranes. A wide variety of precursor polymer membranes can be used. Polyacrylonitrile, poly(vinylidene chloride), poly(furfuryl alcohol), and PIs easily carbonize and have been widely used. As the precursor membrane is heated, there is a gradual loss of weight. The amount and composition of the material lost depends on the polymer. Most polymers lose 10–20 wt% of their weights when the polymer has been heated to 300–500 °C. At this point, the polymer starts the pyrolysis by releasing backbone hydrogens and becomes yellow to brown. Heating at higher temperatures produces more weight loss, and most polymers lose their heteroatoms by the time the polymer reaches 800–1000 °C. During this carbonization process, the membrane usually becomes compact and pores are generated in most cases [162].

1.5.3 Membrane Technology

An overview of membrane technologies is given in Table 1.2. MF, UF, nanofiltration (NF), RO, and ED are well-established technologies. The pressure-driven membrane separation processes of RO, NF, UF, and MF are illustrated in Figure 1.14. The relative size of different solutes removed by each class of membrane is given. RO, NF, UF, MF, and conventional filtration are similar processes differing mainly in the average pore diameter of the membrane. The

Table 1.2 Industrial membrane technologies.

No.	Category	Process
1	Membrane separation technologies well established in the industries	MF, UF, RO, ED
2	Upcoming membrane separation technologies for the industries	Gas separation, pervaporation
3	Membrane separation technologies of interest for the industries	Carrier-facilitated transport membrane contactors, piezodialysis, etc.

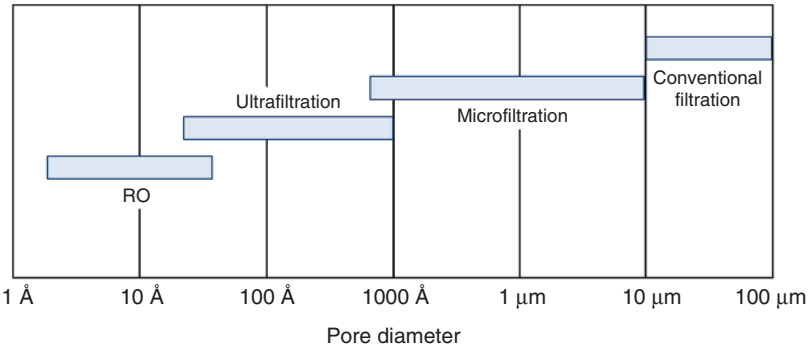

Figure 1.14 Pressure-driven membrane separation processes.

mode of separation in case of NF, UF, and MF is molecular sieving through increasingly fine pores. MF membranes filter colloidal particles and bacteria from 0.1 to 10 μm in diameter. UF membranes can be used to filter dissolved macromolecules, such as proteins from solutions. NF membranes have pore sizes from 1.0 to 10 nm, which is used most often with low total dissolved solids water such as surface water and fresh groundwater, with the purpose of softening and removal of disinfection by-product precursors. MF, UF, and NF membranes are supposed to contain a series of cylindrical capillary pores of specific diameters.

RO membranes are so dense that discrete pores do not exist. Transport occurs through the statistically distributed free volume areas. The pores of the membrane range from 3.0 to 5.0 Å in diameter, which is within molecular level. The mechanism of transport through the RO membrane is governed by the solution–diffusion model. According to this model, solutes permeate the membrane by dissolving in the membrane material and diffusing down a concentration gradient. Separation occurs because of the difference in solubilities and mobilities of different solutes in the membrane.

Table 1.2 shows gas separation and PV as upcoming membrane technologies. Gas separation with membranes has higher potential of application. Several companies worldwide use membrane-based gas separation systems for a variety of applications. In gas separation, a gas mixture at an elevated pressure is transported across the surface of a membrane that is selectively permeable to one component of the feed mixture. Major current applications of gas separation membranes are the separation of hydrogen from nitrogen, argon, and methane in ammonia plants, the production of nitrogen from air, and the separation of carbon dioxide from methane in natural gas operations. In PV, a liquid mixture is fed in the membrane system, and permeate in the form of vapor is removed. The driving force for the process is pressure drop across the membrane. The separation obtained is proportional to the rate of permeation of the particular component through the selective membrane. PV offers the possibility of separating closely boiling mixtures or azeotropes that are difficult to separate by distillation or other means. Currently, the main industrial application of PV technology is for the dehydration of organic solvents, such as the dehydration of 90–95% ethanol

solutions, which is a difficult separation problem because of the ethanol/water azeotrope at 95% ethanol. PV membranes that selectively permeate water can produce more than 99.9% ethanol from these solutions. PV processes are also being developed for the removal of dissolved organics from water and for the separation of organic mixtures.

A number of other industrial membrane processes such as carrier-facilitated transport are under development, which often employs liquid membranes containing a complexing or carrier agent. The carrier agent reacts with one component of a mixture on the feed side of the membrane and then diffuses across the membrane to release permeate on the product side. The reformed carrier agent then diffuses back to the feed side of the membrane. Thus, the carrier agent acts as a shuttle to selectively transport one component from the feed to the product side of the membrane. Facilitated transport membranes can be used to separate gases. In this case, membrane transport is driven by a difference in the partial pressure across the membrane. Metal ions can also be selectively transported across a membrane, driven by a flow of H^+ or OH^- in the other direction. This process is sometimes called coupled transport. As the carrier-facilitated transport process employs a reactive carrier species, very high membrane selectivity can be achieved. The selectivity is often far larger than the one achieved by other membrane processes. This has maintained interest in facilitated transport for so many years. However, commercial deployment is not yet to be deployed due to challenges faced with respect to (i) the physical instability of the liquid membrane and (ii) the chemical instability of the carrier agent. In recent years, a number of potential solutions to this problem have been developed, which may make carrier-facilitated transport a viable process.

The membrane separation processes described earlier represent the bulk of the industrial membrane separation industry. Another process, dialysis, is used on a large scale in the field of medical application to remove toxic metabolites from the blood in patients suffering from kidney failure. The first successful artificial kidney was based on cellophane (regenerated cellulose) dialysis membranes and was developed in 1945. Over the past 50 years, much advancement has been made. Currently, most artificial kidneys are based on hollow fiber membranes formed into modules having a membrane area of about a square meter ($1.0\,m^2$) to remove urea and other toxic elements. Following the success of the artificial kidney, similar devices were developed to remove carbon dioxide and deliver oxygen to the blood. These so-called artificial lungs are used in surgical procedures during which the patient's lungs cannot function. Another major medical use of membranes is in controlled drug delivery. Controlled drug delivery can be achieved by a wide range of techniques, most of which involve membranes.

1.5.4 Membrane Modules

Membrane plants often require large membrane surface areas to perform the separation required on an industrial scale. Prior to separation, modules are needed for economically and efficiently packaging large areas of membranes. The membranes are cast as flat sheets, tubes, and fine hollow fibers. For accommodating such shapes and structures, different types of membrane modules

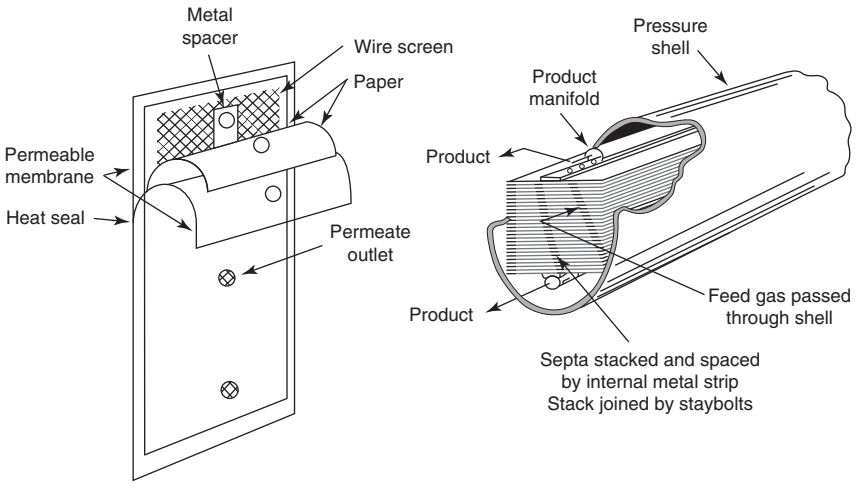

Figure 1.15 An early plate-and-frame design for the separation of helium from natural gas. Source: Reproduced with permission from Reference [163], Copyright John Wiley & Sons.

including plate-and-frame, tubular, spiral wound, and hollow fiber modules have been widely developed for industrial purposes [163].

1.5.4.1 Plate-and-Frame Module

Plate-and-frame modules (Figure 1.15) are one of the earliest types of membrane configuration, in which membrane, feed spacers, and product spacers are layered between two end plates [163, 164]. The feed is sent across the surface of the membrane. A portion of it passes through the membrane, enters the permeate channel, and makes its way to a central permeate collection manifold. Plate-and-frame modules are used in ED and PV systems. A modified version of plate-and-frame module known as disk and tube module configuration has become a popular approach for treating wastewater with highly fouling feed streams.

1.5.4.2 Tubular Membrane Module

Tubular modules are generally applied in MF and UF. The biggest benefit of this module is the high resistance to membrane fouling due to good fluid hydrodynamics. However, the high cost is the main drawback. Typically, the tubes consist of a porous paper or fiberglass support with the membrane on the inside of the tubes. In a typical tubular membrane system, a large number of tubes are arranged in series. The permeate stream from each tube is collected in the permeate collection header. A tubular system is shown in Figure 1.16 [163].

1.5.4.3 Spiral Wound Module

In the spiral wound module, the support fabric, feed spacer, and permeate carrier encase the membrane, providing structural integrity, as shown in Figure 1.17 [163]. Feed solution passes across the membrane surface. A portion passes through the membrane and enters the membrane envelope where it spirals inward to the central perforated collection pipe. The feed enters the module. The

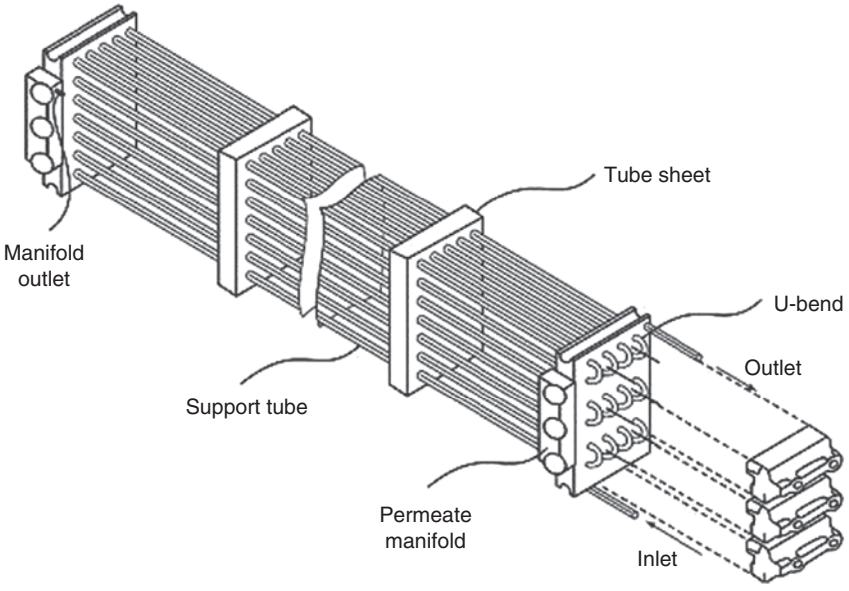

Figure 1.16 A tubular UF membrane system in which tubes are connected in series. Source: Reproduced with permission from Reference [163], Copyright John Wiley & Sons.

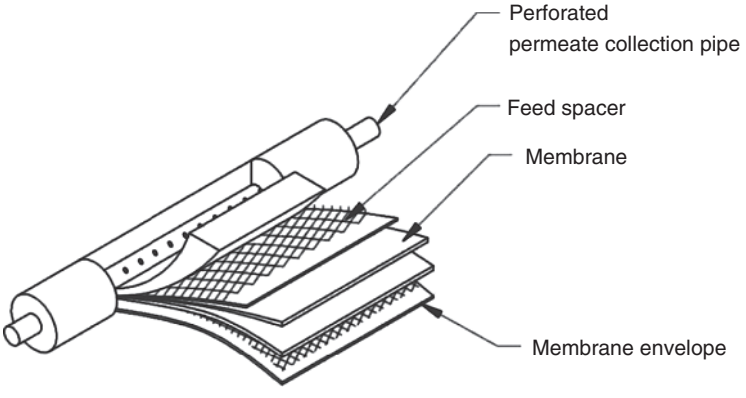

Figure 1.17 An unfolded view of a spiral wound module. Source: Reproduced with permission from Reference [163], Copyright John Wiley & Sons.

permeate stream and concentrate (reject) stream come out of the module. Spiral wound modules are commonly used by desalination industries for brackish and seawater desalination.

1.5.4.4 Hollow Fiber Module

Hollow fiber membrane modules can be classified into two categories based on feed arrangement. The first is the shell-side feed design illustrated in Figure 1.18a [163]. In such a module, a loop or a closed bundle of fibers is contained in a pressure vessel. The system is pressurized from the shell side and the permeate passes

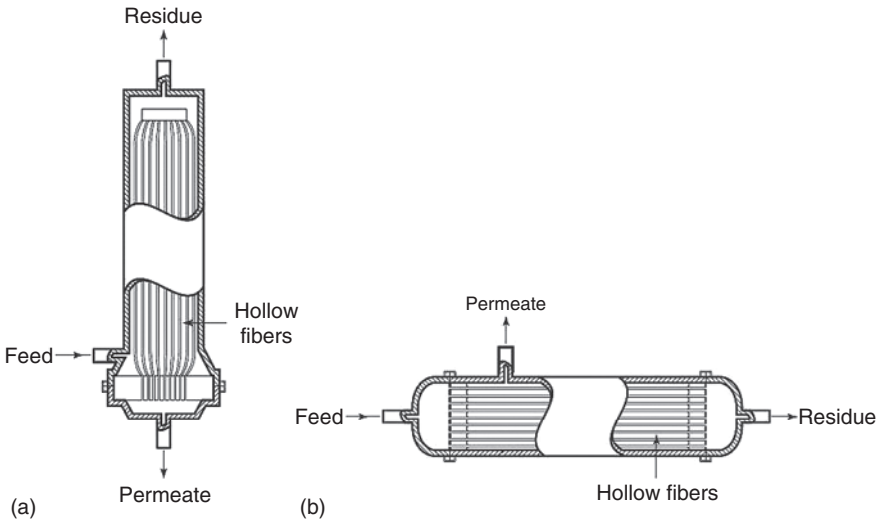

Figure 1.18 Two types of hollow fiber modules: (a) shell-side feed and (b) bore-side feed. Source: Reproduced with permission from Reference [163], Copyright John Wiley & Sons.

through the hollow fiber. Because the fiber wall must support considerable hydrostatic pressure, the fibers usually have small diameters and thick walls, typically 50 and 100–200 μm for respective inner and outer diameters.

The second type of hollow fiber module is the bore-side feed type illustrated in Figure 1.18b. The fibers in this type of unit are open at both ends, and the feed fluid is circulated through the bore of the fibers. To minimize the pressure drop inside the fibers, the diameters are usually larger than those of the fine fibers used in the shell-side feed system. The hollow fibers are generally made by solution spinning. The modules are popular for UF and PV operations. They are used for low- to medium-pressure gas applications. Feed pressures are usually limited to below 10 bars in this type of module. Capillary fiber, which is a modified version of hollow fiber, appears promising for several applications where concentration polarization and fouling are faced in hollow fiber modules.

1.6 Features of Microporous Membranes

In contrast to dense membranes, microporous membranes endow the porous nature. That means membrane materials possess large free volumes and open pores. Figure 1.19 illustrates the most important parameters of microporous materials for membrane application.

The features of microporous membrane are elucidated from the perspective of pore chemistry because this chemistry plays a central role in membrane separation. The pore properties can be determined using the terms of pore size, configuration, dimensionality, and functionality. Pore configuration describes the shapes and connectivity modes of pores. Conforming to the IUPAC recommendation [165], pores that have continuous connection pathways with the

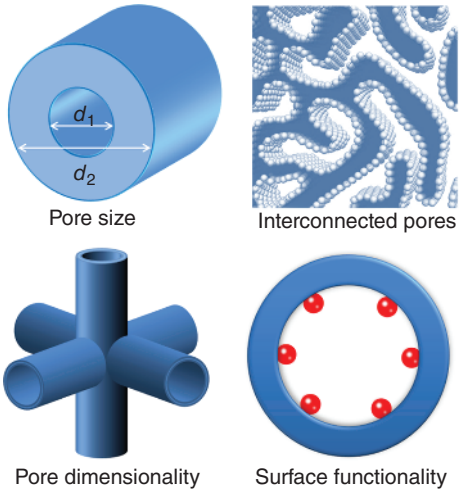

Figure 1.19 Four important parameters – pore size, interconnected pores, pore dimensionality, and surface functionality – of microporous materials for membrane application.

outer surfaces of the porous structure are called open pores. On the other hand, pores that are detached from other pores are called closed pores. The open pores play a pivotal role in fluid dynamics and gas adsorption. From application-based perspectives, materials chemists are interested in open pores. The existence of open pores is prerequisite for separations because interconnected pores form a free pathway for gases or liquids to pass through. The advantage of highly connected pore system is the significant contribution to high permeability or flux. Many microporous materials exhibit interconnected pore configuration because of their uniform pore structures or crystalline phases. For example, zeolites discussed in this book possess well-ordered pores, and the pores are cylinder straight or crossing connected. The occurrence of open pores in zeolites is ascribed to their crystalline phases with all atoms placed regularly in the lattice. For microporous membranes, pore sizes are usually in the range of 3–20 Å. Pore size poses different constraints on molecular diffusions through the pores. According to Lennard-Jones plot [166], a huge potential is measured in micropores. As consequence, smaller molecules diffuse faster than larger ones since there is less hindrance for small molecules. Thus, this effect can be utilized to sieve a particular molecule of interest with good selectivity. After a survey of microporous materials, it can be found that their pores are in the range of 3–20 Å, for instance, zeolites have pores in sizes of 3–14 Å, MOFs own pores in 3–20 Å, CNTs have defined channels of 5–10 Å, etc. Pore dimensionality sometimes also influences the behavior of mass transport. For instance, in a porous membrane with 3D pore systems, a molecule is able to diffuse into the pores easily and subsequently to pass through the membrane in each direction. In contrast, elaborative control on the pore orientation should be made in order to render molecules pass along the 1D channel. The effect of pore dimensionality was in detail investigated by random- and *b*-oriented MFI zeolite membranes [167]. Most of pores are blocked or unused for mass transport in random-oriented membranes. However, great enhancement in xylene flux was achieved by *b*-oriented MFI zeolite membranes. The functionality on the

pore surface is another important parameter that determines the membrane separation performance. The functional groups on the bodies can impose either attractive or repulsive forces toward a particular molecule in the mixture. For example, the adsorption of CO_2 molecules is favored on pore surfaces with high polarities because of the strong van der Waals interactions between CO_2 molecules and polar groups. The result of preferred adsorption is an increase in the adsorption selectivity and consequently an enhancement to the overall separation selectivity. The strong interaction also facilitates the close packing of CO_2 molecules along the pore wall, which eventually increases CO_2 permeability in the process of membrane separation. The influence of functionality in separation performance was symmetrically studied by MOF membranes in gas separations [122]. A variety of functionalities such as unsaturated metal centers in clusters, amino groups on ligands, and polar OH entities were introduced in order to improve CO_2 selectivity in MOF material-based membranes. From the above basics, it can be concluded that pore chemistry is of vital importance in membrane separation.

1.7 Conclusions

This chapter has made short introductions in a wide span of subjects. In the beginning, we have introduced the basics of membranes, and then we reviewed the original membranes to the most recent modern membranes. A particular attention has been paid to microporous materials including nomenclature, types, and structures of carbon, silica, zeolite, MOF, and porous organic polymer. This overview can help us to understand microporous materials comprehensively from materials perspective. In parallel, fundamentals of membrane separation have been discussed in depth, including separation theory, membrane configuration, membrane fabrication, and membrane module. This discussion can help us to comprehend the separation process from the point of view of membrane engineering. In the end, we were closely looking at the features of microporous membranes, which would play a central role in membrane-based separations. We hope all the basics in this chapter provide a solid platform for our dear readers to digest other chapters more easily and offer a solution to equip us with rich knowledge.

References

1 Baker, R.W. (2004). *Membrane Technology and Applications*, 2e. Menlo Park, CA: Membrane Technology and Research Inc.
2 Bechhold, H. (1907). *Z. Phys. Chem.* 60: 257.
3 Elford, W.J. (1937). *Trans. Faraday Soc.* 33: 1094.
4 Zsigmondy, R. and Bachmann, R. (1918). *Z. Anorg. Chem.* 103: 119.
5 Ferry, J.D. (1936). *Chem. Rev.* 18: 373.
6 Loeb, S. and Sourirajan, S. Sea water demineralization by means of an osmotic membrane. In: *Saline Water Conversion-II*, Advances in Chemistry

Series Number, 1963, vol. 38 (ed. R.F. Gould), 117–132. Washington, DC: American Chemical Society.
7 Kolf, W.J. and Berk, H.T. (1944). *Acta Med. Scand.* 117: 121–134.
8 Henis, J.M.S. and Tripodi, M.K. (1980). *Sep. Sci. Technol.* 15: 1059–1068.
9 de Vos, R.M. and Verweij, H. (1998). *Science* 279: 1710–1711.
10 Freni, A., Dawoud, B., Bonaccorsi, L. et al. (2015). *Characterization of Zeolite-Based Coatings for Adsorption Heat Pumps*. Springer.
11 Wright, P.A. and Connor, J.A. (eds.) (2007). *Microporous Framework Solids*, 1e. Royal Society of Chemistry.
12 IUPAC (1972). *Pure Appl. Chem.* 31: 577–638.
13 Romanos, J., Beckner, M., Rash, T. et al. (2012). *Nanotechnology* 23: 015401.
14 Yang, R.T. (2003). *Adsorbents: Fundamentals and Applications*, 208–213. Wiley.
15 Mendez-Linan, L., Lopez-Garzon, F.J., Domingo-Garcia, M., and Perez-Mendoza, M. (2010). *Energy Fuel* 24: 3394–3400.
16 Serp, P. and Figueiredo, J.L. (2009). *Carbon Materials for Catalysis*, 550. Wiley.
17 (a) Gómez-Serrano, V., Piriz-Almeida, F., Durán-Valle, C.J., and Pastor-Villegas, J. (1999). *Carbon* 37: 1517–1528. (b) Machnikowski, J., Kaczmarska, H., Gerus-Piasecka, I. et al. (2002). *Carbon* 40: 1937–1947. (c) Petrov, N., Budinova, T., Razvigorova, M. et al. (2000). *Carbon* 38: 2069–2075. (d) Garcia, A.B., Martinez-Alonso, A., Leon, C.A., and Tascon, J.M.D. (1998). *Fuel* 77: 613–624. (e) Polovina, M., Babic, B., Kaluderovic, B., and Dekanski, A. (1997). *Carbon* 35: 1047–1052. (f) Fanning, P.E. and Vannice, M.A. (1993). *Carbon* 31: 721–730. (g) Youssef, A.M., Abdelbary, E.M., Samra, S.E., and Dowidar, A.M. (1991). *Indian J. Chem.* 30: 839–843.
18 (a) Arriagada, R., Garcia, R., Molina-Sabio, M., and Rodriguez-Reinoso, F. (1997). *Microporous Mater.* 8: 123–130. (b) Molina-Sabio, M., Gonzalez, M.T., Rodriguez-Reinoso, F., and Sepulveda-Escribano, A. (1996). *Carbon* 34: 505–509. (c) Bradley, R.H., Sutherland, I., and Sheng, E. (1996). *J. Colloid Interface Sci.* 179: 561–569.
19 Saha, B., Tai, M.H., and Streat, M. (2001). *Process Saf. Environ.* 79: 211–217.
20 (a) Sutherland, I., Sheng, E., Braley, R.H., and Freakley, P.K. (1996). *J. Mater. Sci.* 31: 5651–5655. (b) Rivera-Utrilla, J. and Sanchez-Polo, M. (2002). *Carbon* 40: 2685–2691. (c) Valdés, H., Sánchez-Polo, M., Rivera-Utrilla, J., and Zaror, C.A. (2002). *Langmuir* 18: 2111–2116.
21 (a) Pradhan, B.K. and Sandle, N.K. (1999). *Carbon* 37: 1323–1332. (b) Acedo-Ramos, M., Gomez-Serrano, V., Valenzuella-Calahorro, C., and Lopez-Peinado, A.J. (1993). *Spectrosc. Lett.* 26: 1117–1137. (c) Gomez-Serrano, V., Acedo-Ramos, M., Lopez-Peinado, A.J., and Valenzuela-Calahorro, C. (1991). *Thermochim. Acta* 176: 129–140.
22 (a) Stőhr, B., Boehm, H.P., and Schlőgl, R. (1991). *Carbon* 29: 707–720. (b) Biniak, S., Szymański, G., Siedlewski, J., and Światkowski, A. (1997). *Carbon* 35: 1799–1810.
23 (a) Boudou, J.P., Chehimi, M., Broniek, E. et al. (2003). *Carbon* 41: 1999–2007. (b) Radkevich, V.Z., Senko, T.L., Wilson, K. et al. (2008). *Appl. Catal. A Gen.* 335: 241–251.

24 (a) Evans, M.J.B., Halliop, E., Liang, S., and MacDonald, J.A.F. (1998). *Carbon* 36: 1677–1682. (b) Papirer, E.N., Lacroix, R., Donnet, J.B. et al. (1995). *Carbon* 33: 63–72.

25 Papirer, E., Lacroix, R., Donnet, J.B. et al. (1994). *Carbon* 32: 1341–1358.

26 Nansé, G., Papirer, E., Fioux, P. et al. (1997). *Carbon* 35: 515–528.

27 Aldana-Pérez, A., Lartundo-Rojas, L., Gómez, R., and Niño-Gómez, M.E. (2012). *Fuel* 100: 128–138.

28 Diyuk, V.E., Zaderko, A.N., Grishchenko, L.M. et al. (2012). *Catal. Commun.* 27: 33–37.

29 Budarin, V.L., Clark, J.H., Tavener, S.J., and Wilson, K. (2004). *Chem. Commun.* 2736–2737.

30 EPA Alumni Association. Senior EPA officials discuss early implementation of the Safe Drinking Water Act of 1974.

31 Iijima, S. (1991). *Nature* 354: 56–58.

32 Lalwani, G., Kwaczala, A.T., Kanakia, S. et al. (2013). *Carbon* 53: 90–100.

33 Lalwani, G., Gopalan, A., D'Agati, M. et al. (2015). *J. Biomed. Mater. Res. A* 103: 3212–3225.

34 Takeuchi, K., Hayashi, T., Kim, Y.A. et al. (2014). *Nanosystems: Phys. Chem. Math.* 5: 15–24.

35 Karousis, N., Tagmatarchis, N., and Tasis, D. (2010). *Chem. Rev.* 110: 5366–5397.

36 Yu, M.F., Lourie, O., Dyer, M.J. et al. (2000). *Science* 287: 637–640.

37 Peng, B., Locascio, M., Zapol, P. et al. (2008). *Nat. Nanotechnol.* 3: 626–631.

38 Filleter, T., Bernal, R., Li, S., and Espinosa, H.D. (2011). *Adv. Mater.* 23: 2855–2860.

39 Wang, Z.K., Ci, L.J., Chen, L. et al. (2007). *Nano Lett.* 7: 697–702.

40 Lu, X. and Chen, Z. (2005). *Chem. Rev.* 105: 3643–3696.

41 Hong, S. and Myung, S. (2007). *Nat. Nanotechnol.* 2: 207–208.

42 Charlier, J.C. and Roche, S. (2007). *Rev. Mod. Phys.* 79: 677–732.

43 Haddon, R.C., Laura, P.Z., Bin, Z., and Hui, H. (2006). *Nano Lett.* 6: 562–567.

44 Reibold, M., Paufler, P., Levin, A.A. et al. (2006). *Nature* 444: 286.

45 Liu, F., Wagterveld, R.M., Gebben, B. et al. (2014). *Colloid. Interface Sci. Comm.* 3: 9–12.

46 Pyrhönen, J., Montonen, J., Lindh, P. et al. (2015). *Int. Rev. Electr. Eng.* 10: 12.

47 Cooper, D.R., D'Anjou, B., Ghattamaneni, N. et al. (2012). *ISRN Condens. Matter Phys.* 501686.

48 Geim, A. (2009). *Science* 324: 1530–1534.

49 Kusmartsev, F.V., Wu, W.M., Pierpoint, M.P., and Yung, K.C. (2014). *Condens. Matter. Mater. Sci.* 14060809.

50 Geim, A.K. and MacDonald, A.H. (2007). *Phys. Today* 60: 35–41.

51 Jayasena, B. and Subbiah, S. (2011). *Nanoscale Res. Lett.* 6: 95.

52 Eigler, S., Enzelberger-Heim, M., Grimm, S. et al. (2013). *Adv. Mater.* 25: 3583–3587.

53 El-Kady, M.F., Strong, V., Dubin, S., and Kaner, R.B. (2012). *Science* 335: 1326–1330.

54 Hernandez, Y., Nicolosi, V., Lotya, M. et al. (2008). *Nat. Nanotechnol.* 3: 563–568.
55 Alzari, V., Nuvoli, D., Scognamillo, S. et al. (2011). *J. Mater. Chem.* 21: 8727–8733.
56 Nuvoli, D., Valentini, L., Alzari, V. et al. (2011). *J. Mater. Chem.* 21: 3428–3431.
57 Woltornist, S.J., Oyer, A.J., Carrillo, J.M.Y. et al. (2013). *ACS Nano* 7: 7062–7066.
58 Bointon, T.H., Barnes, M.D., Russo, S., and Craciun, M.F. (2015). *Adv. Mater.* 27: 4200–4206.
59 Das, S. and Drucker, J. (2017). *Nanotechnology* 28: 10.
60 Chiu, P.L., Mastrogiovanni, D.D.T., Wei, D. et al. (2012). *J. Am. Chem. Soc.* 134: 5850–5856.
61 Patel, M., Feng, W., Savaram, K. et al. (2015). *Small* 11: 3358–3368.
62 Li, Z., Chen, L., Meng, S. et al. (2015). *Phys. Rev. B* 91: 094429.
63 Bonaccorso, F., Colombo, L., Yu, G. et al. (2015). *Science* 347: 41–52.
64 Avouris, P., Chen, Z., and Perebeinos, V. (2007). *Nat. Nanotechnol.* 2: 605–615.
65 (a) Novoselov, K.S., Geim, A.K., Morozov, S.V. et al. (2005). *Nature* 438: 197–200. (b) Morozov, S.V., Novoselov, K., Katsnelson, M. et al. (2008). *Phys. Rev. Lett.* 100: 016602. (c) Chen, J.H., Jang, C., Xiao, S. et al. (2008). *Nat. Nanotechnol.* 3: 206–209.
66 Akturk, A. and Goldsman, N. (2008). *J. Appl. Phys.* 103: 053702.
67 Bernardo, A.D., Millo, O., Barbone, M. et al. (2017). *Nat. Commun.* 8: 14024.
68 Baringhaus, J., Ruan, M., Edler, F. et al. (2014). *Nature* 506: 349–354.
69 Neto, A.C., Peres, N.M.R., Novoselov, K.S., and Geim, A.K. (2009). *Rev. Mod. Phys.* 81: 109–162.
70 Chen, J.H., Jang, C., Adam, S. et al. (2008). *Nat. Phys.* 4: 377–381.
71 Schedin, F., Geim, A.K., Morozov, S.V. et al. (2007). *Nat. Mater.* 6: 652–655.
72 Adam, S., Hwang, E.H., Galitski, V.M., and Das, S.S. (2007). *Proc. Natl. Acad. Sci.* 104: 18392–18397.
73 Steinberg, H., Barak, G., Yacoby, A. et al. (2008). *Nat. Phys.* 4: 116–119.
74 Trisetyarso, A. (2012). *Quantum Inf. Comput.* 12: 989.
75 Pachos, J.K. (2009). *Contemp. Phys.* 50: 375–389.
76 Balandin, A.A., Ghosh, S., Bao, W. et al. (2008). *Nano Lett.* 8: 902–907.
77 (a) Cai, W., Moore, A.L., Zhu, Y. et al. (2010). *Nano Lett.* 10: 1645–1651. (b) Faugeras, C., Faugeras, B., Orlita, M. et al. (2010). *ACS Nano* 4: 1889–1892. (c) Xu, X., Pereira, L.F.C., Wang, Y. et al. (2014). *Nat. Commun.* 5: 3689. (d) Lee, J.U., Yoon, D., Kim, H. et al. (2011). *Phys. Rev. B* 83: 081419.
78 Denis, P.A. and Iribarne, F. (2013). *J. Phys. Chem. C* 117: 19048–19055.
79 Yamada, Y., Murota, K., Fujita, R. et al. (2014). *J. Am. Chem. Soc.* 136: 2232–2235.
80 Eftekhari, A. and Jafarkhani, P. (2013). *J. Phys. Chem. C* 117: 25845–25851.
81 Yamada, Y., Yasuda, H., Murota, K. et al. (2013). *J. Mater. Sci.* 48: 8171–8198.
82 Yamada, Y., Kim, J., Murota, K. et al. (2014). *Carbon* 70: 59–74.
83 Dissanayake, D.M.N.M., Ashraf, A., Dwyer, D. et al. (2016). *Sci. Rep.* 6: 21070.

84 Zhong, M., Xu, D., Yu, X. et al. (2016). *Nano Energy* 28: 12–18.
85 Akinwande, D., Tao, L., Yu, Q. et al. (2015). *IEEE Nanotechnol. Mag.* 9: 6–14.
86 (a) Lalwani, G., Henslee, A.M., Farshid, B. et al. (2013). *Biomacromolecules* 14: 900–909. (b) Rafiee, M.A., Rafiee, J., Wang, Z. et al. (2009). *ACS Nano* 3: 3884–3890.
87 Shehzad, K., Xu, Y., Gao, C., and Duan, X. (2016). *Chem. Soc. Rev.* 45: 5541–5588.
88 Barboiu, C., Sala, B., Bec, S. et al. (2009). *J. Membr. Sci.* 326: 514–525.
89 Ayral, A., Julbe, A., Rouessac, V. et al. (2008). Microporous silica membrane: basic principles and recent advances. In: *Membrane Science and Technology* (ed. M. Reyes and M. Miguel), 33–79. Elsevier: Amsterdam.
90 Tsuru, T. (2003). *Porous Ceramics for Filtration, Handbook of Advanced Ceramics*, 291–312. Oxford: Academic Press.
91 Nair, B.N., Elferink, W.J., Keizer, K., and Verweij, H. (1996). *J. Colloid Interface Sci.* 178: 565–570.
92 Witoon, T., Tatan, N., Rattanavichian, P., and Chareonpanich, M. (2011). *Ceram. Int.* 37: 2297–2303.
93 Naito, M., Nakahira, K., Fukuda, Y. et al. (1997). *J. Membr. Sci.* 129: 263–269.
94 Kanezashi, M. and Tsuru, T. (2011). Gas permeation properties of helium, hydrogen, and polar molecules through microporous silica membranes at high temperatures: correlation with silica network structure. In: *Membrane Science and Technology* (ed. S.T. Oyama and M.S.W. Susan), 117–136. Elsevier: Amsterdam.
95 Lin, Y.S., Kumakiri, I., Nair, B.N., and Alsyouri, H. (2002). *Sep. Purif. Rev.* 31: 239–248.
96 Wang, X., Miao, X.R., Li, Z.M., and Deng, W.L. (2011). *Appl. Surf. Sci.* 257: 2481–2488.
97 Eswaramoorthy, M., Neeraj, S., and Rao, C.N.R. (1999). *Microporous Mesoporous Mater.* 28: 205–210.
98 Guo, L., Dong, X., Cui, X. et al. (2009). *Mater. Lett.* 63: 13–14.
99 Raman, N.K. and Brinker, C.J. (1995). *J. Membr. Sci.* 105: 273–279.
100 Labropoulos, A.I., Romanos, G.E., Karanikolos, G.N. et al. (2009). *Microporous Mesoporous Mater.* 120: 177–185.
101 Breck, D.W. (1974). *Zeolite Molecular Sieves: Structure, Chemistry, and Use*. New York: Wiley.
102 Cronstedt, A.F. (1993). Observations and descriptions on an unknown mineral species called zeoloites. *Proceedings of 9th International Zeolite Conference* (ed. R. van Ballmoos, J.B. Higgins, and H.M.J. Treacy), 3–9. Boston: Butterworth-Heinemann.
103 Deville, H.d.S.C. (1862). *C. R. Seances Acad. Sci.* 54: 324.
104 Wadlinger, R.L., Kerr, G.T., and Rosinski, E.J. (1967). Catalytic composition of a crystalline zeolite. US Patent 3308069.
105 (a) Barrer, R.M. (1978). *Zeolites and Clay Minerals as Sorbents and Molecular Sieves*. London: Academic Press. (b) Barrer, R.M. (1982). *Hydrothermal Chemistry of Zeolites*. London: Academic Press.

106 (a) Plank, C.J. and Rosinski, E.J. (1964). Process for carbonizing coal. US Patent 3140240; (b) Breck, D.W. (1964). Crystalline zeolite y. US Patent 31300007; (c) Biswas, J. and Maxwell, I.E. (1990). *Appl. Catal.* 63: 197–258.

107 (a) Argauer, R.J. and Landolt, G.R. (1972). Crystalline zeolite ZSM-5 and method of preparing the same. US Patent 3702886; (b) Flanigen, E.M., Bennett, J.M., Grose, R.W. et al. (1978). *Nature* 271: 512–516. (c) Szostak, R. (1992). *Handbook of Molecular Sieves*. New York: Springer.

108 (a) Wilson, S.T., Lok, B.M., Messina, C.A. et al. (1982). *J. Am. Chem. Soc.* 104: 1146–1147. (b) Flanigen, E.M., Patton, R.L., and Wilson, S.T. (1988). *Stud. Surf. Sci. Catal.* 37: 13–27.

109 International Zeolite Association (2007). *Atlas of Zeolite Framework Types*, 6ee. http://www.iza-online.org.

110 Rollmann, L.D. and Valyocsik, E.W. (1995). Zeolite molecular sieves. In: *Inorganic Syntheses: Nonmolecular Solids*, vol. 30 (ed. D.W. Murphy and L.V. Interrante), 227–234. Wiley.

111 Earl, D.J. and Deem, M.W. (2006). *Ind. Eng. Chem. Res.* 45: 5449–5454.

112 Auerbach, S.M., Carrado, K.A., and Dutta, P.K. (2003). *Handbook of Zeolite Science and Technology*. New York: Marcel Dekker Inc.

113 Cheetham, A.K., Férey, G., and Loiseau, T. (1999). *Angew. Chem. Int. Ed.* 38: 3268–3292.

114 (a) Bucar, D.K., Papaefstathiou, G.S., Hamilton, T.D. et al. (2007). *Eur. J. Inorg. Chem.* (29): 4559–4568. (b) Parnham, E.R. and Morris, R.E. (2007). *Acc. Chem. Res.* 40: 1005–1013.

115 Wang, Z. and Cohen, S.M. (2009). *Chem. Soc. Rev.* 38: 1315–1329.

116 (a) Dincă, M. and Long, J.R. (2008). *Angew. Chem. Int. Ed.* 47: 6766–6779. (b) Das, S., Kim, H., and Kim, K. (2009). *J. Am. Chem. Soc.* 131: 3814–3815.

117 Pichon, A. and James, S.L. (2008). *CrystEngComm* 10: 1839–1847.

118 Murray, L.J., Dincă, M., and Long, J.R. (2009). *Chem. Soc. Rev.* 38: 1294–1314.

119 Czaja, A.U., Trukhan, N., and Müller, U. (2009). *Chem. Soc. Rev.* 38: 1284–1293.

120 Mendoza-Cortés, J.L., Han, S.S., and GoddardIII, W.A. (2012). *J. Phys. Chem. A* 116: 1621–1631.

121 Choi, S., Drese, J.H., and Jones, C.W. (2009). *ChemSusChem* 2: 796–854.

122 Sumida, K., Rogow, D.L., Mason, J.A. et al. (2012). *Chem. Rev.* 112: 724–781.

123 Millward, A.R. and Yaghi, O.M. (2005). *J. Am. Chem. Soc.* 127: 17998–17999.

124 Berger, A.H. and Bhown, A.S. (2011). *Energy Procedia* 4: 562–567.

125 Masuda, T. (2007). *J. Polym. Sci., Part A: Polym. Chem.* 45: 165–180.

126 Grubbs, R.H. (ed.) (2003). *Handbook of Metathesis*. Weinheim: Wiley-VCH.

127 (a) Nagai, K., Masuda, T., Nakagawa, T. et al. (2001). *Prog. Polym. Sci.* 26: 721–797. (b) Aoki, T. (1999). *Prog. Polym. Sci.* 24: 951–993. (c) Ulbricht, M. (2006). *Polymer* 47: 2217–2262. (d) Freeman, B.D., Yampolskii, Y., and Pinnau, I. (eds.) (2006). *Materials Science of Membranes for Gas and Vapor Separation*. Chichester: Wiley.

128 (a) Finkelshtein, E.S., Makovetskii, K.L., Gringolts, M.L. et al. (2006). *Macromolecules* 39: 7022–7029. (b) Starannikova, L., Pilipenko, M., Belov, N. et al. (2008). *J. Membr. Sci.* 323: 134–143.

129 Kim, J.F. and Drioli, E. (2016). Perfluoropolymers in membranes. In: *Encyclopedia of Membranes* (ed. E. Drioli and L. Giorno), 1479–1480. Springer.

130 Anolick, C., Hrivnak, J.A., and Wheland, R.C. (1998). *Adv. Mater.* 10: 1211–1214.

131 Liaw, D.J., Wang, K.L., Huang, Y.C. et al. (2012). *Prog. Polym. Sci.* 37: 907–974.

132 (a) Tanaka, K., Okano, M., Toshino, H. et al. (1992). *J. Polym. Sci. B Polym. Phys.* 30: 907–914. (b) Liu, Y., Pan, C., Ding, M., and Xu, J. (1999). *Polym. Int.* 48: 832–836. (c) Lin, W.H., Vora, R.H., and Chung, T.S. (2000). *J. Polym. Sci. B Polym. Phys.* 38: 2703–2713.

133 Park, H.B., Jung, C.H., Lee, Y.M. et al. (2007). *Science* 318: 254–258.

134 (a) Feng, X., Ding, X.S., and Jiang, D.L. (2012). *Chem. Soc. Rev.* 41: 6010–6022. (b) Ding, S.Y. and Wang, W. (2013). *Chem. Soc. Rev.* 42: 548–568. (c) Cooper, A.I. (2009). *Adv. Mater.* 21: 1291–1295. (d) Thomas, A. (2010). *Angew. Chem. Int. Ed.* 49: 8328–8344. (e) Zou, X.Q., Ren, H., and Zhu, G.S. (2013). *Chem. Commun.* 49: 3925–3936.

135 Côté, A.P., Benin, A.I., Ockwig, N.W. et al. (2005). *Science* 310: 1166–1170.

136 El-Kaderi, H.M., Hunt, J.R., Mendoza-Cortés, J. et al. (2007). *Science* 316: 268–272.

137 Uribe-Romo, F.J., Hunt, J.R., Furukawa, H. et al. (2009). *J. Am. Chem. Soc.* 131: 4570–4571.

138 Shun, W., Jia, G., Jangbae, K. et al. (2008). *Angew. Chem. Int. Ed.* 47: 8826–8830.

139 (a) Kuhn, P., Forget, A., Su, D. et al. (2008). *J. Am. Chem. Soc.* 130: 13333. (b) Kuhn, P., Antonietti, M., and Thomas, A. (2008). *Angew. Chem. Int. Ed.* 47: 3450.

140 Palkovits, R., Antonietti, M., Kuhn, P. et al. (2009). *Angew. Chem. Int. Ed.* 48: 6909.

141 Zhang, Y. and Riduan, S.N. (2012). *Chem. Soc. Rev.* 41: 2083–2094.

142 McKeown, N.B., Makhseed, S., and Budd, P.M. (2002). *Chem. Commun.* 2780–2781.

143 (a) Eastmond, G.C. and Paprotny, J. (1999). *Chem. Lett.* 479–480. (b) Eastmond, G.C., Paprotny, J., Steiner, A., and Swanson, L. (2001). *New J. Chem.* 25: 379–384.

144 (a) Budd, P.M., Ghanem, B.S., Makhseed, S. et al. (2004). *Chem. Commun.* 230–231. (b) Budd, P.M., Elabas, E.S., Ghanem, B.S. et al. (2004). *Adv. Mater.* 16: 456–459.

145 Budd, P.M. and McKeown, N.B. (2010). *Polym. Chem.* 1: 63–68.

146 Ben, T., Ren, H., Ma, S. et al. (2009). *Angew. Chem. Int. Ed.* 48: 9457–9460.

147 Ben, T., Pei, C., Zhang, D. et al. (2011). *Energy Environ. Sci.* 4: 3991–3999.

148 Ben, T. and Qiu, S. (2013). *CrystEngComm* 15: 17–26.

149 Ren, H., Ben, T., Wang, E. et al. (2010). *Chem. Commun.* 46: 291–293.

150 (a) Ben, T., Shi, K., Cui, Y. et al. (2011). *J. Mater. Chem.* 21: 18208–18214. (b) Meng, S., Zou, X.Q., Liu, C.F. et al. (2016). *ChemCatChem* 8: 2393–2400.

151 Inzelt, G. (2008). *Conducting Polymers: A New Era in Electrochemistry*. Berlin, Heidelberg: Springer.

152 Liu, Q., Tang, Z., Wu, M., and Zhou, Z. (2014). *Polym. Int.* 63: 381–392.

153 Boucle, J., Ravirajan, P., and Nelson, J. (2007). *J. Mater. Chem.* 17: 3141–3153.

154 Kluiters, S.C.A. (2004). Status review on membrane system for hydrogen separation. Intermediate Report EU Project MIGREYD NNE5-2001-670.

155 Ghosh, A.K. (2003). Ultrafiltration membrane. PhD thesis, Bombay University, Mumbai, India.

156 Siemann, U. (2005). Solvent cast technology – a versatile tool for thin film production. In: *Progress in Colloid and Polymer Science*, vol. 130 (ed. C. Papadakis, A.M. Schmidt and F. Kremer), 1–14. Springer.

157 Mackenzie, K.J. (1992). Film and sheeting material. In: *Encyclopedia of Chemical Technology*, 4e, vol. 10 (ed. Kirk-Othmer), 761. Hoboken, NJ: Wiley.

158 Ziabicki, A. (1976). *Fundamentals of Fiber Formation*. London: Wiley.

159 Schubert, D.W. and Dunkel, T. (2003). *Mater. Res. Innov.* 7: 314–321.

160 (a) Li, K. (2007). *Ceramic Membranes for Separation and Reaction*. Chichester: Wiley. (b) Keizer, K., Uhlhorn, R.J.R., and Burggraaf, T.J. (1995). Gas separation using inorganic membranes. In: *Membrane Separation Technology, Principles and Applications* (ed. R.D. Noble and S.A. Stern), 553–584. Amsterdam: Elsevier. (c) Burggraaf, T.J. and Keizer, K. (1991). Synthesis of inorganic membranes. In: *Inorganic Membranes Synthesis, Characteristics, and Applications* (ed. R.R. Bhave), 10–63. New York: Chapman & Hall.

161 (a) Larbot, A., Fabre, J.P., Guizard, C., and Cot, L. (1988). *J. Membr. Sci.* 39: 203–212. (b) Anderson, M.A., Gieselmann, M.J., and Xu, Q. (1988). *J. Membr. Sci.* 39: 243–258.

162 Ismail, A.F. and Salleh, W.N.W. (2013). Carbon membranes. In: *Encyclopedia of Membrane Science and Technology* (ed. E.M.V. Hoek and V.V. Tarabara), 1–29. Inc.: Wiley.

163 Baker, R.W. (2004). Membranes and modules. In: *Membrane Technology and Applications*, 89–160. Wiley.

164 Stern, S.A., Sinclaire, T.F., Gareis, P.J. et al. (1965). *Ind. Eng. Chem.* 57: 49–60.

165 Rouquerol, J., Avnir, D., Fairbridge, C.W. et al. (1994). *Pure Appl. Chem.* 66: 1739–1758.

166 Lennard-Jones, J.E. (1924). *Proc. R. Soc. Lond. A* 106: 463–477.

167 Snyder, M.A. and Tsapatsis, M. (2007). *Angew. Chem. Int. Ed.* 46: 7560–7573.